Nano Today 25 (2019) 68–84

Contents lists available at ScienceDirect

Nano Today

journal homepage: www.elsevier.com/locate/nanotoday

Review

# Exploiting lanthanide-doped upconversion nanoparticles with core/shell structures

Yong Fan [1], Lu Liu [1], Fan Zhang *

*Department of Chemistry, Shanghai Key Laboratory of Molecular Catalysis and Innovative Materials, State Key Laboratory of Molecular Engineering of Polymers and iChem, Fudan University, Shanghai, 200433, PR China*

ARTICLE INFO

*Article history:*
Received 13 November 2018
Received in revised form 18 January 2019
Accepted 26 February 2019
Available online 10 March 2019

*Keywords:*
Lanthanide ions
Upconversion
core/shell
Nanomaterials
Multifunctionality

ABSTRACT

Lanthanide-doped upconversion nanoparticles (UCNPs) are guest-host systems with lanthanide ions as guest dispersed in a dielectric material as the inorganic host. Over the past decades, much efforts have been devoted to UCNPs in a number of biological applications due to their low toxicity, high chemical stability and high signal-to-noise ratio. Lanthanide ions distributed in conventional UCNPs with only core structures easily lose their excitation and emission energy through energy migration to the surface quenchers, weakening the emission intensities. A hierarchically designed core/shell structure may address the challenges above by blocking the emitters from the surface and surrounding quenchers. Besides, it offers not only a flexible construction by employing active shells to endow the UCNPs with new features from enhanced light harvesting and multicolor tunability to therapeutic functions, but also largely preserves the optical integrity of UCNPs. In this review, we primarily focus on recent progress in the hierarchically designed core/shell UCNPs and discussing their challenges and opportunities. We summarize several strategies to synthesize and characterize the core/shell structure and particularly highlight the unprecedented properties through regulating the core/shell structure, including light harvesting, tuning of excitation wavelength, enhancement of emission efficiency, emission color tunability, lifetime tunability and multifunctionality. Finally, we frame the future outlook of challenges and opportunities for core/shell UCNPs.



**Contents**



* Corresponding author.
*E-mail address:* zhang_fan@fudan.edu.cn (F. Zhang).
[1] These two authors contributed equally to this work.

https://doi.org/10.1016/j.nantod.2019.02.009
1748-0132/

## Introduction

Lanthanide-doped nanoparticles via intra-4f or 4f-5d transitions have received considerable attention due to the benefit of sharp-band emissions, long fluorescence lifetime, excellent stability against photobleaching as well as multiple emission bands from ultra violet (UV) to infrared (IR) by single wavelength excitation, and have enabled a broad range of applications in background-less biological sensing, light-triggered drug delivery, solar energy harvesting and super-resolution microscopy [1–6]. Not only downshifting (Stokes type) but also upconversion (anti-Stokes type) luminescence can arise in these nanoparticles [7–9]. Upconversion luminescence (UCL) is a non-linear optical process, in which at least two low-energy photons with long wavelength (generally from IR region) are absorbed via physically existing intermediate long-lived energy states, followed by the emission of one high-energy photon with shorter wavelength than the absorbed ones. Unlike other multi-photon absorption strategies such as second-harmonic generation (SHG) [10–12] and two-photon absorption (TPA) [13–15], the sequential absorption of multiple photons in lanthanide upconverion offers the advantage of using much lower excitation power density which can be easily realized by low cost continuous-wave laser.

UC phenomenon was discovered in 1960s and the investigations has primarily been limited to bulk glass or crystalline materials until the late 1990s, when upconversion nanoparticles (UCNPs) appeared and has captured worldwide attention thanks to the development of nanoscience and nanotechnology [16–18]. However, due to the large surface area of UCNPs, nonradiative channels associated with the impurities and surface defects deactivate the UCL intensity to a large extent [19,20]. Besides, interactions between lanthanide ions depended on the doping process also play a key role in modulating the brightness of UCNPs. Moreover, the limited excitation light harvesting ability and the excitation wavelength tunability due to the nature of 4f-4f transition of lanthanide ions fundamentally restrict their quantum yield (QY) as compared to that of organic dyes and quantum dots (QDs). Despite their promising applications in many area [1–6], all the above disadvantages of UCNPs inhibit their UC brightness as well as functionalities and restrict their further practical applications from bench to clinical practice.

Nevertheless, rational design of the UCNPs with size, composition, nanostructure as well as surface properties may address the challenges above, among which constructing core/shell UCNPs is one of the effective ways. Inspired by the idea of taking advantage of a shell on QDs to minimize the influence of nonradiative transitions from the particle surface [21–23], the core/shell structure designed on UCNPs provides boosted UCL efficiencies by growing protection shells as well. With the development of nanochemistry, the shell layers can subsequently be regulated within a defined scale as well as a stoichiometric composition. Besides, core/shell nanostructural engineering introduces a new variable into materials design by constructing UCNPs with homogeneous or heterogeneous shells, thereby offering substantial flexibility for synergistically offering new multifunctions and tunable properties in a broad application range from bioimaging to therapy, while conserving all the merits of conventional UCNPs.

In this review, we systematically summarize the recent progress focusing on the hierarchically designed core/shell UCNPs and discuss their challenges and opportunities. Rational control of the core/shell UCNPs is essential for obtaining optimal optical properties, thus we first provide several strategies for synthesizing high-quality core/shell UCNPs with well-defined size, tunable shell thickness and compositions. Then we present a series of approaches to characterize the presence of a core/shell structure. Furthermore, the effects of engineering core/shell UCNPs on several aspects are discussed, including light harvesting, tuning of excitation wavelength, enhancement of emission efficiency, emission color tunability, lifetime tunability and multifunctionality (Fig. 1). Finally, we frame the future outlook of challenges and opportunities for the preparation, characterization as well as application of core/shell UCNPs.

## Constructing UCNPs with core/shell structures

Hitherto, chemical synthetic approaches, including thermal decomposition, hydro(solvo)thermal synthesis, sol-gel processing and ionic liquid-based synthesis, have been demonstrated to synthesize high-quality core only UCNPs. Optimization of the synthesis procedure is crucial to obtain nanocrystals with suitable particle size, morphology, and optical performance. To further monipulate the optical properties and provide an excellent platform to combine different functional units into one single nanoparticle, UCNPs with core/shell structures offer operability and diversity, which opens up new opportunities for various applications [1,24,25]. Up to now, several strategies have been adopted to construct UCNPs with core/shell structures (Table 1) and readers may also refer to those recently published reviews for more detailed information [3,26,27].

### *Seed-mediated heat-up method*

Seed-mediated heat-up method is one of the most widely used approaches to prepare high quality core/shell structure UCNPs with a relatively uniform morphology and size. In this strategy, the core of UCNPs must exists first and is utilized as seed nuclei for the epitaxial growth of the outer shell layer (Fig. 2a). In particular, the concentration of shell precursor needs to be low in regard to the concentration of the core of UCNPs to avoid the homogeneous nucleation of the shell host material alone rather than formation of the core/shell UCNPs. During the procedure, the shell thickness can be adjusted by controlling the molar ratio of core to shell precursor. In addition, to ensure an epitaxial growth with a homogeneous morphology, the lattice match should be considered between the host material of the shell and that of the core material. Otherwise, heterogeneous morphology of the shell will be formed. Based on this method, many UCNPs with core/shell structures have been designed for various applications, such as $EuF_3$@$GdF_3$ [28], $NaYF_4$@$NaYF_4$ [29], $NaYbF_4$@$CaF_2$ [30], $NaGdF_4$@$NaGdF_4$ [31], and $LiLuF_4$@$LiLuF_4$ [32]. Except for lattice match, the size and morphology of core/shell structures are also affected by the heating rate, reaction temperature, time, precursor concentration [33].

### *Ostwald ripening strategy*

Ostwald ripening is based on the process by growing larger particles at sacrifice of the smaller ones, which are less ener-

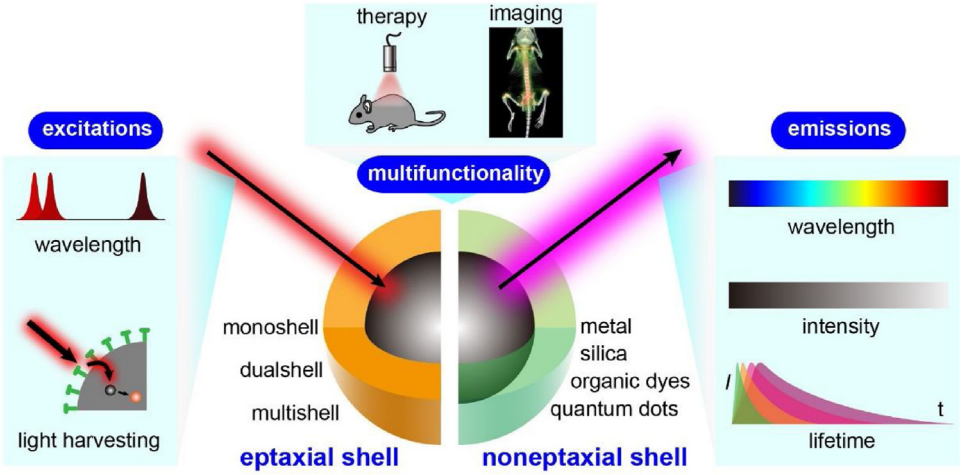


**Fig. 1.** Schematic illustrations of tunable effects on upconversion nanoparticles with core/shell structures.

**Table 1**
Typical synthetic routes to UCNPs with core/shell structures.

| Method | Advantages | Drawbacks | References |
|---|---|---|---|
| Seed-mediated heat-up | nanoparticles with relatively uniform morphology and size, narrow size distribution | time-consuming, laborious, user unfriendly, low lattice mismatch between core and shell material is needed for obtaining uniform homogeneous interface | [19,20,28,29,30,31,32,33,36,37,38,39,49,51,58,64,65,71,73,74,76,77,78,79,80,82,83,88,91,92,93,94,97,99,100,101,102,114,115,116,117,118,119,120,121,126,135,136,139,147,148], |
| Ostwald Ripening | flexible, nanoparticles with well defined shape, narrow size distribution, tunable shell growth | time-consuming, laborious, sacrificial nanoparticles are needed, low lattice mismatch between core and shell material is needed for obtaining uniform homogeneous interface | [34,35,62,63,96,134,136] |
| Successive layer-by-layer | flexible to deposit uniform multishells, able to precisely control shell thickness on both hexagonal and cubic phase cores | time-consuming when thick shell is designed | [5,38,40,41,42,60,61,72,130,137,138] |
| Cation exchange reaction | convenient, rapid sample synthesis, constructing core/shell structure with maintained size, moderate experimental conditions, reduced solvent and reagent consumption | ineffective to precisely control the exchanging parts, non-uniform shell | [43–45] |
| Nonepitaxial growth | multifunctions | complicated synthesis procedures, non-uniform shell | [4,42,46,47,48,49,50,51,52,53,54,55,56,57,59,84,95,106,107,129,141,148,149] |

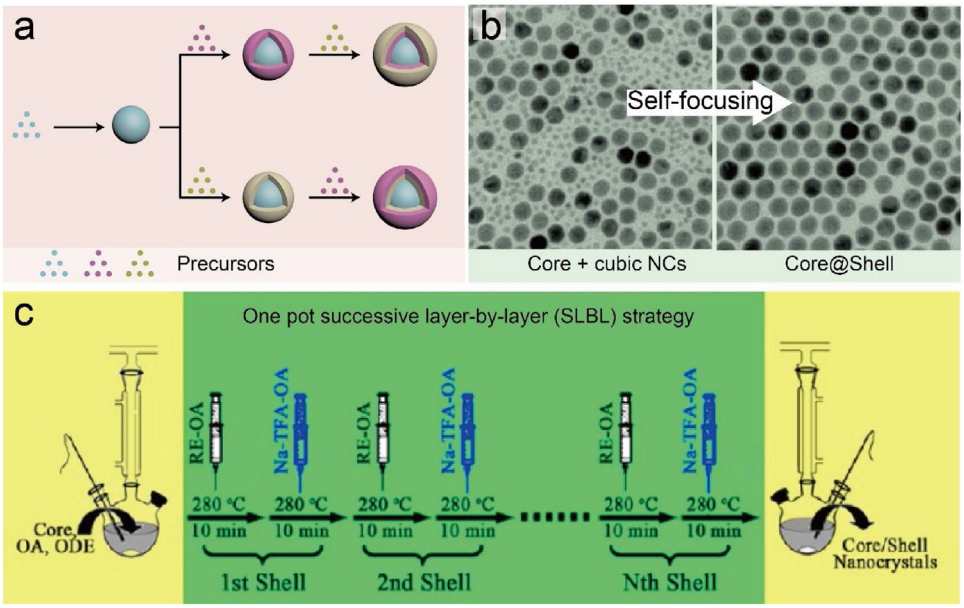


**Fig. 2.** (a) One pot strategy of heat-up of pre-synthesized core nanoparticles with varying shell precursors. (b) Self-focusing method obtained by injection of small sacrificial nanoparticles [34]. Printed with permission from American Chemical Society. (c) One pot successive layer-by-layer (SLBL) synthetic procedure for the core/shell UCNPs [40]. Printed with permission from American Chemical Society.

getically stable due to the higher surface to volume ratio. When shell monomers, dissolved from the α-phase sacrificial nanoparticles, are supersaturated, the free monomers tend to deposit on the larger stable core nanoparticles. Therefore, all smaller particles shrink, while larger particles grow to form the core/shell structures. This method has been successfully applied to grow $NaYF_4$ shell on the $NaYF_4$:Yb/Er core nanoparticles, and the resulted core/shell nanoparticles showed high-quality homogeneous morphology with uniform size (Fig. 2b) [34]. Although almost identical TEM images and X-ray powder diffraction data were obtained in fabrication of $NaEuF_4/NaGdF_4$ core/shell nanoparticles with high quality, the degree of intermixing of core and shell material were slightly different in the seed-mediated heat-up method and Ostwald ripening strategy, which can be determined by means of optical spectroscopy [35]. Besides, this intermixing can be decreased by optimizing the synthesis parameters of shell formation.

*Successive layer-by-layer method*

Although widely used, a non-uniform shell may also appear using the seed-mediated heat-up method [36–38], and bimodal size distribution was always observed when a high volume of shell precursors was introduced [39]. Besides, this method is considered to be time-consuming, laborious and user unfriendly, especially for the synthesis of UCNPs with multishells. Therefore, a protocol of one pot successive layer-by-layer (SLBL) deposition was developed which offered a facile way for constructing UCNPs with uniform multishells (Fig. 2c) [40]. In this work, shell thickness of the obtained UCNPs with narrow size distribution ($\sigma < 10\%$) can be well controlled from 0.36 nm to more than 8 nm by simply tuning the amounts of shell precursors. By changing the injection rate of shell precursors and keeping all the other reaction conditions constant, shell morphologies can also be tuned [41,42]. While isotropic shell growth were observed for fast sequential injection, shell growth along the crystal's c-axis [001] were preferred when adopting slow dropwise-injection [41]. Similar to the seed-mediated heat-up method, the monomer concentration also needs to keep low during the growth process to suppress homogeneous nucleation. With the SLBL method, high quality core/shell UCNPs with multifunctional structure can be synthesized, which may provide a new strategy to manipulate the UCNPs in nanoscale.

*Cation exchange reaction*

Cation exchange reaction is another facile way to prepare monodisperse core/shell UCNPs. The cations at the UCNPs surface and in the reaction solution exchange reversibly, leading to the formation of a unique heterogeneous shell layer on the inner core without concerning variation in particle size, phase and morphology. One of the earliest examples of this method was adopted to synthesize the $GdF_3$@$LnF_3$ core/shell nanoparticles by exposing the $GdF_3$ core to citrate aqueous solution containing excess $Ln^{3+}$ ions [43]. By refining this synthetic route, multifunctional $NaYF_4$:Yb/Tm@$NaGdF_4$ core/shell UCNPs with tunable shell thickness, enhanced UCL and outstanding paramagnetic performance could also be prepared easily [44]. Recently, a large class of UCNPs were realized with various emitters based on this strategy, which opens a gateway towards applications ranging from chemical sensing to anti-counterfeiting [45]. In particular, this approach allows the development of a general, green protocol for preparing multicolor nanoprobes or nanomaterials that cannot be made directly, combining efficient and rapid sample synthesis with significantly reduced solvent and reagent consumption.

*Nonepitaxial growth*

Multifunctional nanocomposites have recently attracted more and more attention. Through appropriately tailoring the core/shell nanoplatform with nonepitaxial shells, new functions can be incorporated into the UCNPs, which can extend the scope of their potential applications. Noble metals can be assembled on the surface of UCNPs to modulate their UCL through plasmonic interactions. For example, ligand-exchange process was first carried out to render the UCNPs positively charged by using poly(acrylic acid) (PAA) and poly(allylamine hydrochloride) (PAH). Then negatively charged gold nanoparticles can be attached on the surface of UCNPs. To grow a continuous gold shell, the gold nanoparticles can act as the nucleation seeds in additional gold precursors [46]. In another report, CdSe QDs were dendritically decorated on the surface of $NaYF_4$:Yb/Er nanoparticles in organic solvents. The driven force was considered to be the electrostatic attraction between the different ligands on the surface of QDs (amine-capped) and UCNPs (acid capped) [47].To expand the UCNPs in wide biological and biomedical applications, silica or mesoporous silica ($mSiO_2$) shells can be encased due to their well-developed surface chemistry and morphology. Common strategies of coating silica include reverse microemulsion method, Stöber method and so on [48,49]. UCNP@$SiO_2$@$mSiO_2$ nanospheres and PMO single-crystal nanocubes have been successfully synthesized via a novel anisotropic island nucleation and growth approach with the ordered mesostructure [50]. In addition to the aforementioned core/shell nanoparticles, a large variety of multifunctional nanocomposites, such as magnetic nanoparticles, metal and semiconductor nanocomposites etc., have also been prepared [51–57].

## Characterization of core/shell nanostructures

Compared to the homogeneously doped nanoparticles with limited scope, core/shell nanostructure engineering has brought new functionalities and a powerful means to regulate the optical properties of the nanoparticles. Therefore, investigating the integrity of a core/shell nanostructure is one of the key roles. The characterization techniques for investigation of a core/shell structure conventionally include scanning electron microscopy (SEM), transmission electron microscopy (TEM), high-angle annular dark-field (HAADF) scanning transmission electron microscopy (STEM), X-ray photoelectron spectroscopy (XPS), energy-dispersive X-ray spectroscopy (EDS), electron energy loss spectroscopy (EELS), photoluminescence (PL), photoluminescence lifetime, dynamic light scattering (DLS). These characterization strategies have also been reviewed in some excellent review articles [3,26,27] and we here mainly focus on the basic principles of each method with some discussions. Depending on the different characteristics, those techniques can be classified into two sections.

*Direct evidence of core/shell nanostructures*

SEM is useful to directly reveal the state of nanoparticle surface and in general cannot be able to 'see inside'. However, only in some special morphology, such as a porous shell or a core-satellite structure, has it possible to verify the successful shell and core part (Fig. 3a) [58]. When the core and the shell matrix are not the same in composition and crystallinity as in heterogonous epitaxial core/shell UCNPs, various characterization techniques can be adopted to study the structural morphology. TEM is one of the most common and reliable techniques and discerns the core/shell structures through the good contrast between the core and shell [59]. This method can also be utilized in nonepitaxial core/shell UCNPs. To further determine the position of atoms, the crystallinity, lattice

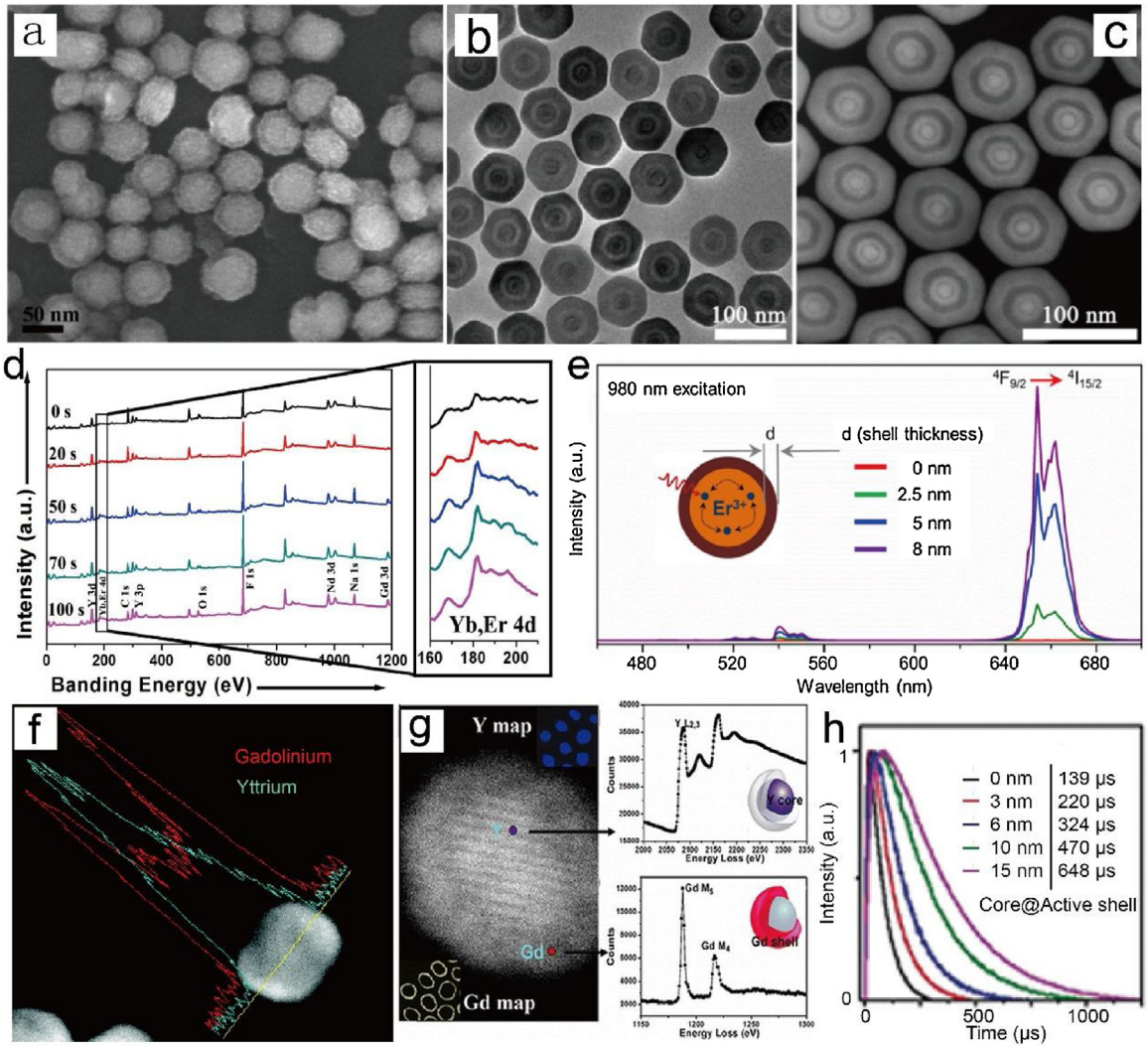


**Fig. 3.** (a) SEM images of mUCNPs: $NaYbF_4$:2%Er@$NaGdF_4$ [58]. Printed with permission from Elsevier B.V. (b, c) TEM and HAADF-STEM images of the core-quadruple shell structured nanoparticles [60]. Printed with permission from Wiley-VCH. (d) XPS spectra of core/Shell/shell/shell nanocrystals under argon ion bombardment at different bombardment time [61]. Printed with permission from Wiley-VCH. (e) Upconversion emission spectra of $NaErF_4$ core and $NaErF_4$-$NaLuF_4$ core/shell nanocrystals with increasing shell thickness [62]. Printed with permission from American Chemical Society. (f) EDS line scan across a single $NaYF_4$-$NaGdF_4$ core/shell NC showing Y in the core of the particle and Gd located in the shell [37]. Printed with permission from American Chemical Society. (g) EELS spectra of yttrium $L_{2,3}$ and gadolinium $M_{4,5}$ edges taken from the probe location on the inferred $NaYF_4$:Yb,Er core and $NaGdF_4$ shell [38]. Printed with permission from American Chemical Society. (h) Shell thickness dependent 540 nm UC emission decay lifetime of the core-active shell structures [63]. Printed with permission from Wiley-VCH.



fringes, and even the d-spacing of the core/shell structures, high-resolution TEM (HRTEM) is usually adopted with higher working voltage. HAADF imaging takes advantages of the contrast, which scales proportionally to the atomic number of the elements in the core and the shell, to distinguish the heterogeneous epitaxial core/shell structure. For example, Li et al. demonstrated the formation of core-quadruple shell nanostructure in which the Gd-rich domain appears bright (Z = 64) and Y-rich domain appears dark (Z = 39) (Fig. 3b and c) [60]. Although attractive, this technique is only useful when the atomic number between the core and shell matrix is large enough. XPS is an important technique to reveal the surface information of the nanoparticles, in which the analyte depths in the nanoparticles can be estimated. Therefore, it can also be utilized to conform a core/shell structure by studying the intensity of main elements (Fig. 3d) [61]. Note that, this is an ensemble measurement and does not show any individual structure details. Compared to the above characterizations based on imaging, EDS and EELS are two element mapping techniques for obtaining chemical composition of individual nanoparticle to distinguish a core/shell structure. While EDS is particularly sensitive to heavier elements, EELS tends to work best at relatively light elements, which exhibits quick and reliable measurement of local shell thickness. Abel et al. [37] and Zhang et al. [38] employed these techniques to successfully demonstrate the formation of the $NaYF_4$@$NaGdF_4$ and $NaYF_4$:Yb,Er@$NaGdF_4$ core/shell structures, respectively, according to the intensity ratio between the yttrium peak and the gadolinium peak across a single particle (Fig. 3f and g). The disadvantage of this method, however, is the long acquisition times for line scans to confirming the shell distribution around the nanocrystal, which may result in considerable beam damage. Although all the present techniques are able to provide direct evidence of the formation of a core/shell structure, adequate characterizations strategy or the combinations are need to be considered depending on situations.

*Indirect evidence of core/shell nanostructures*

Properties like electron, size, luminescence, lifetime, or electron diffraction from materials are the major research objects for nanoparticle characterization either in the colloidal state or in the powder form. Comparing the above physical and chemical characteristics between the core only and core/shell nanostructures, the formation of a core/shell structure can also be indicated indirectly. In the case of homogeneous epitaxial core/shell UCNPs, where the core and shell matrix have the same composition, TEM analysis can also be adopted as an indirect protocol to confirm the shell growth by showing the nanoparticle size increase, accompanied by narrowing of XRD peaks. Besides, the enhancement of luminescence (Fig. 3e) [62], different intensity ratio of red-to-green emission, as well as the variance of photoluminescence lifetime (Fig. 3h) [63], can be achieved by introducing a shell layer on the core of UCNPs, meaning a successful core/shell structure. By combining the time-resolved and steady-state luminescence of $Ce^{3+}$ and $Tb^{3+}$ in $NaYF_4$:20%Ce@$NaYF_4$:20%Tb nanoparticles, the integrity of core/shell structures can also be validated [64]. The reasons above can be attributed to the elimination of the surface quenchers and constructing energy migration channel at the core/shell interface, respectively. In addition, DLS is an effective physical technique that can be used to determine the size distribution of small particles, which can be used to indicate the shell growth by measuring the average size of the nanoparticles both in core only and core/shell form [65]. Nevertheless, the limitation of all the above indirect characterization ways is that they do not provide structural details of the shell layer.

## Effect of Lanthanide doped nanoparticles with core/shell structure

UCL is a nonlinear optical phenomenon and its underlying physical origins, such as excited state absorption (ESA), energy transfer upconversion (ETU), cooperative sensitization upconversion (CSU), photon avalanche (PA) and energy migration upconversion (EMU), have been extensively studied both theoretically and experimentally [2,39,66–70]. With the advances of materials chemistry, core/shell structures offer a facile way to decently engineer the distribution of lanthanide ions spatially and can be designed with substantial flexibility. As a consequence, core/shell structures can not only realize desirable excitation light harvesting, tunable excitation wavelength, and emission wavelengths manipulation as well as UC lifetime and efficiency, but also offer an integrated platform for introducing multifunctionalities, which has shown vast applications in various field from bioimaging to biological therapy.

*Enhancement of light harvesting*

Due to the intraconfigurational dipole-dipole forbidden nature of 4f-4f transitions, the extinction coefficient and absorption band of lanthanide ions are lower than organic dyes, giving rise to extremely weak light absorption of UCNPs, especially when the size of UCNP is down to nanoscale range. These unfavorable features as well as the deleterious surface-related quenching effects (eg. surface defects, high-energy vibrations of solvent and/or ligand molecules) will inevitably engender a low emission efficiency of UCNPs with core only and limit their applications in bioimaging when excited with a low-intensity laser source. Enhancing the light harvesting will address the absorption issue aforementioned from the root, which can be effectively implemented through constructing core/shell structures by introducing extra absorbers. In general, two strategies can be commonly adopted to fulfill the need. The first is to introduce extra lanthanide absorbers in the shell, and the second is to coupling UCNPs with organic dye shell in nature with higher absorption coefficient and a broad absorption band.

As the most widely used sensitizer, ytterbium ion ($Yb^{3+}$) is able to sensitize common emitters ($Er^{3+}$, $Ho^{3+}$ and $Tm^{3+}$) to produce UCL due to its large absorption cross-section in the NIR region (~980 nm). However, there is a constraint in dopant concentrations in the conventional $Yb^{3+}$/emitter codoped system, in which optimal $Yb^{3+}$ is indispensable to obtain efficient UCL rising from the competition effect between elevated absorption capability and deleterious cross-relaxation of $Yb^{3+}$. Therefore, it is impractical to further increase $Yb^{3+}$ concentration to enlarge absorption capability as well as UCL intensity. Thanks to the core/shell structures, this constraint can be overcome by introducing certain amount of $Yb^{3+}$ into the shell (active shell) as extra absorbers to boost the light harvesting (Fig. 4a,b) [31]. This active shell serves two purposes: one is to protect the UCL intensity of emitters from non-radiative decay, especially those near the surface of the core; the other is to transfer the pumping light to the core region to promote the UC process. Inspired by this approach, several other groups have also observed remarkable enhancement in UCL in homogeneous active core/active shell structure such as $BaGdF_5$:Yb,Er@$BaGdF_5$:Yb [71], $BaLuF_5$:Yb,Er@$BaLuF_5$:Yb [72], $KMnF_3$:Yb,Er@$KMnF_3$:Yb [73], $BaYF_5$:Yb,Er@$BaYF_5$:Yb [74], $NaYF_4$:Yb,Er@ $NaYF_4$:Yb [75], $NaYbF_4$:Nd@$NaYF_4$:Yb [76] UCNPs, as well as heterogeneous structures ($CaF_2$:Yb,Tm,Ho@$NaYF_4$:Yb [77]). Similar to the core, concentration quenching also happens in the active shell, meaning optimal amount of $Yb^{3+}$ is need to be performed as well. To reduce this deleterious high-concentration quenching effects and transfer more absorbed NIR energy to the emitters, a recent work reported a core/shell/shell structure by sandwiching the luminescent shell between an active core and an active shell ($NaGdF_4$:Yb@$NaYF_4$:Yb,Er@$NaGdF_4$:Yb), which exhibited increased UCL intensity compared to $NaYF_4$:Yb,Er@$NaGdF_4$:Yb active core-active shell structure [78]. These results demonstrated that active shells played a vital role in light harvesting and thus UCL enhancement.

Apart from doping lanthanide ions as extra absorbers to enhance light harvesting, organic dyes and fluorophores with absorption cross-section three- to four orders larger than that of common sensitizers (e.g. $Yb^{3+}$) as well as wide absorption band have also been applied to UCNPs as antennas [79–84]. It should be noted that these antennas should not only have a reasonable match for the excitation band of the sensitizers in UCNPs, but also need to be far away from the absorption band of the interested UCL, in case of decreasing the UCL intensity through re-absorption. For example, by coupling with organic dyes IR-806 as the antennas (Fig. 4c), the intensity of UC green emission of $\beta$-$NaYF_4$:Yb/Er nanoparticles was enhanced by a factor of ~300 under 975 nm irradiation (Fig. 4d) due to the increased absorptivity and overall broadening of the absorption spectrum [84]. Despite of the dramatic increment of the UCL intensity, the net upconversion quantum yield (UCQY) is still lower than ~0.1%. One of the reasons is that an inefficient energy transfer from the organic dyes to $Yb^{3+}$, owing to the large energy mismatch (~2200 $cm^{-1}$) between them. Moreover, to allow the sensitization of organic dye to occur, bare core nanoparticles without shells have to be used, which will dramatically quench the UCL due to the surface-related defects. To achieve higher UCQY, Chen et al. proposed an energy-cascaded upconversion in a similar hybrid organic-inorganic system consisting of $NaYbF_4$:0.5%Tm@$NaYF_4$:Nd@IR-808 [79]. This structure enables three energy transfer steps (dye→$Nd^{3+}$(shell)→$Yb^{3+}$(core)→$Tm^{3+}$(core)) with small energy gap between each other, thus a high energy transfer efficiency from the organic dye harvester all the way down to the emitters can be expected, which enables UCQY as high as 4.8%. Recently, similar work has also been reported by Wu et al. who developed dye-sensitized $NaYF_4$:Yb,Er@$NaYF_4$:Yb

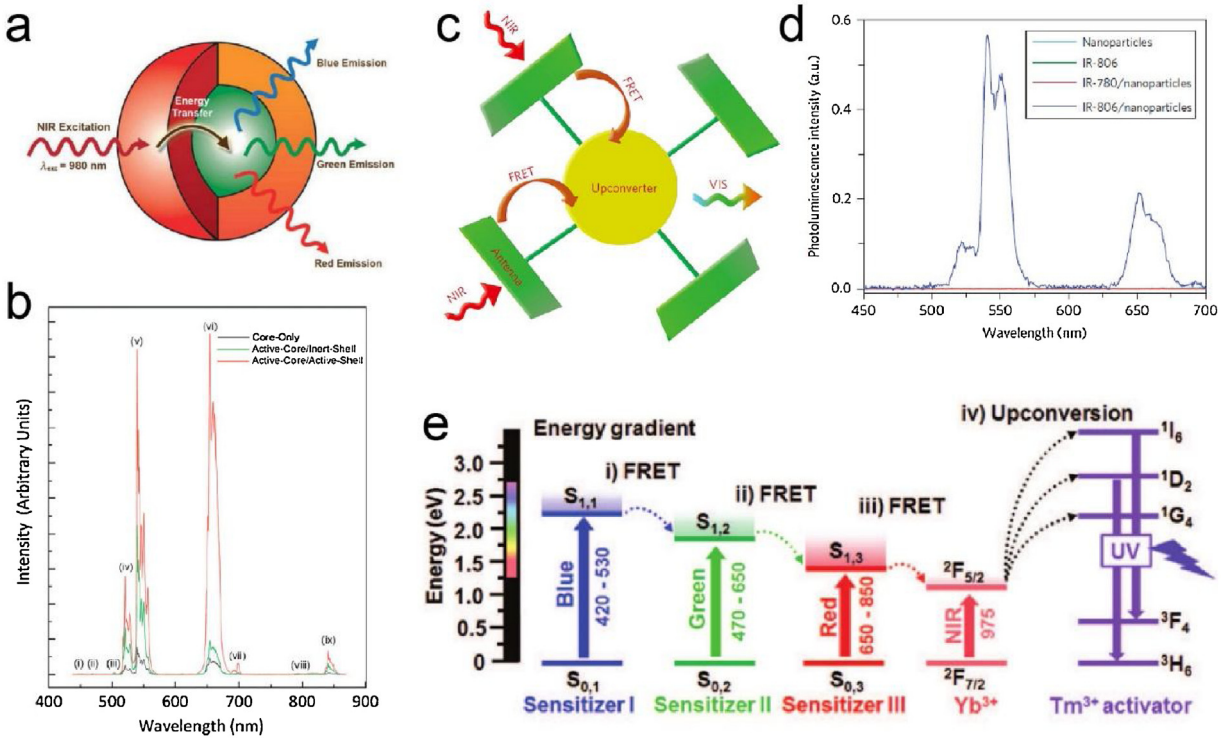


**Fig. 4.** (a) General depiction of the $NaGdF_4$:Er,Yb@$NaGdF_4$:Yb active-core@active-shell nanoparticles under 980 nm excitation [31]. Printed with permission from Wiley-VCH. (b) UC luminescence spectra of colloidal $NaGdF_4$: Yb,Er (core only), $NaGdF_4$:Yb,Er@$NaGdF_4$ (active-core@inertshell) and $NaGdF_4$:Yb,Er@$NaGdF_4$:Yb (active-core@active-shell) nanoparticles in 1 wt% toluene under 980 nm excitation [31]. Printed with permission from Wiley-VCH. (c) Principal concept of the dye-sensitized nanoparticle. Dyes as antenna (green) absorb NIR light (red wavy arrows), which is transferred (brown arrows) to the nanoparticle core (in yellow), where UC occurs [84]. Printed with permission from Nature Publishing Group. (d) UC emission spectra of β-$NaYF_4$:Yb,Er nanoparticles, IR-806, β-$NaYF_4$:Yb,Er nanoparticles@IR-780 and β-$NaYF_4$:Yb,Er nanoparticles@IR-806 in $CHCl_3$ under 800 nm excitation [84]. Printed with permission from Nature Publishing Group. (e) Energy diagram of the three sensitizers (sensitizer I: BODIPY-FL, sensitizer II: Cy3.5, sensitizer III: IR806) sequentially transfer the absorbed energy to the UCNPs ($Tm^{3+}$). The arrows represent the sequential energy transfer [80]. Printed with permission from Wiley-VCH.

Reproduced with permission. Copyright 2009, 2017, Wiley-VCH Verlag GmbH & Co. KGaA, Weinheim; Copyright 2012, Nature Publishing Group.

UCNPs [82]. By doping of $Yb^{3+}$ in the active shell to bridge the energy transfer from the dye to the UCNP core through $Yb^{3+}$ sublattice, the dye-sensitized core/active shell system showed absolute UCQY of ~5% in DMF. Besides, in comparison with dye-sensitized UCNP core ($NaYF_4$:Yb,Er) and dye-sensitized core/inert shell UCNPs ($NaYF_4$:Yb,Er@$NaYF_4$), the UCL intensity of the reported new system enhanced 8 and 70 times, respectively. By rationally employing multi-dyes, ultra-wide absorption band using sequential energy transfer can be implemented on the UCNPs from the NIR to the entire visible range including red, green and blue (Fig. 4e) [80]. This expansion of absorption enables to use diverse initial energies for UC to easily yield a high energy (UV) photon. Through the enhanced light-harvesting ability and well-established functionalization strategies, organic dyes sensitized UCNPs possess not only the improvement of their UCL brightness but also the expanding of versatile applications.

*Tuning of the excitation wavelength*

Although 980 nm absorbed by $Yb^{3+}$ is the most commonly used excitation source to generate UCL, a major limitation of this wavelength for biological applications is its well overlapped region with the absorption peak of water, the most significant component of the animal and human [85]. Therefore, the penetration depth of the laser beam would be very shallow due to the overwhelmingly attenuated light diffusing in biological tissues. Besides, this absorbed light will result in a risk of local temperature rise and substantial overheating under continuous irradiation, hindering the further development of $Yb^{3+}$ sensitized nanocrystals. To address this limitation, excitation wavelengths of UCNPs should be controlled in an appropriate range to minimize the heating effect for wide biological applications. In the last few years, $Nd^{3+}$ has been introduced as a new sensitizer absorbed light at 808 nm, since it situates in the NIR region (700–900 nm) with minimal absorbance for all bio-molecules [85–88]. Different from a single excited state of $Yb^{3+}$, the abundant energy levels of $Nd^{3+}$ may deactivate the emitters ($Ho^{3+}$, $Tm^{3+}$ and $Er^{3+}$) via cross-relaxation rather than sensitize them, although their energy levels overlapped. Tri-doped with $Yb^{3+}$ as the bridging ions can suppress the deleterious effect and transfer the energy from $Nd^{3+}$ to the emitters efficiently due to the high energy transfer efficiency from $Nd^{3+}$ to $Yb^{3+}$ (up to 70%) [89,90] and the commonly efficient $Yb^{3+}$/($Ho^{3+}$, $Tm^{3+}$ and $Er^{3+}$) pairs. Therefore, higher UCL intensity of UCNPs is expected, considering the absorption cross-section of $Nd^{3+}$ at 808 nm is one order higher than that of $Yb^{3+}$ at 980 nm [89]. A cascade sensitized $NaYF_4$:Nd/Yb/Er(Tm)@$NaYF_4$ core/shell UCNPs were successfully demonstrated to be excited at ~800 nm [91]. Nevertheless, the challenge of the tri-doped system is revealed by the deleterious energy back-transfer from $Er^{3+}$ ($Tm^{3+}$) to $^4I_J$ manifolds of $Nd^{3+}$, leading to a lower UCL intensity [92]. To minimize the harsh quenching interactions, the doping concentration of $Nd^{3+}$ can only be constrained below 1%, limiting the light absorption capability and the UC efficiency of this system correspondingly.

To remove the above constraint due to back-energy transfer, spatially separated the emitter and $Nd^{3+}$ in the core and shell, respectively, is the effective strategy. For example, Wang et al. synthesized $NaGdF_4$:Yb/Er@$NaGdF_4$:Nd core/shell UCNPs to shift the conversional excitation wavelength from 980 nm to

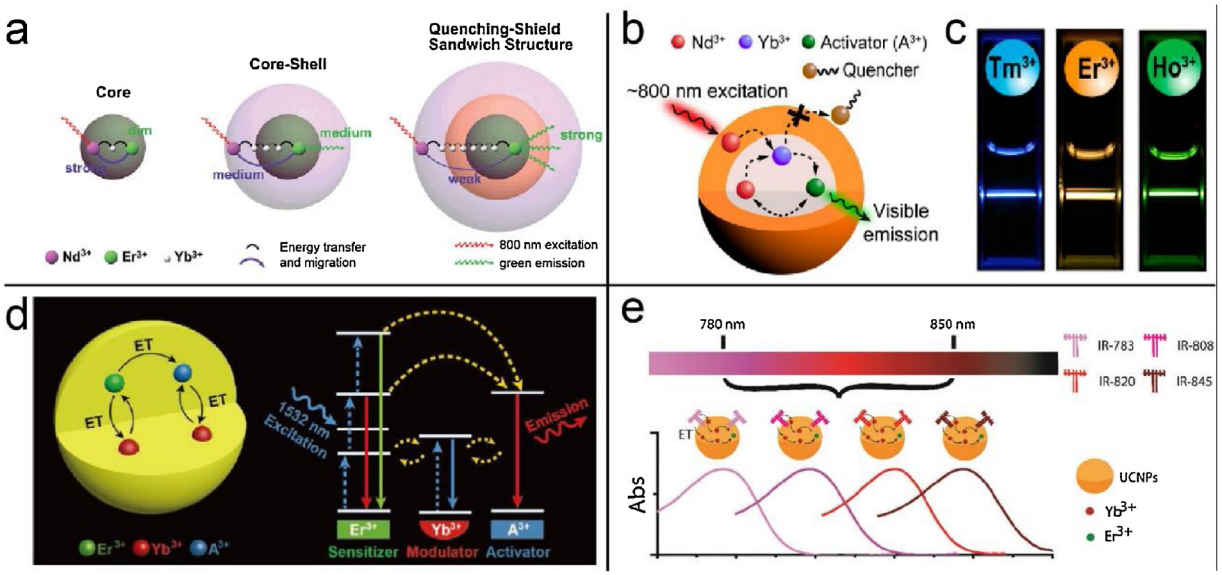


**Fig. 5.** (a) Schematic illustration of the energy-transfer and migration processes in the $NaYF_4$:Nd,Yb,Er core, $NaYF_4$:Yb,Er@$NaNdF_4$ core/shell, and $NaYF_4$:Yb,Er@$NaYF_4$:Yb@$NaNdF_4$:Yb quenching-shield sandwich nanoparticles [92]. Printed with permission from Wiley-VCH. (b) Schematic design and (c) luminescence photographs of the $NaYF_4$:Yb/Nd/X@$NaYF_4$:Nd (X = Tm, Er, Ho) core/shell nanoparticles under 800 nm excitation for photon UC [93]. Printed with permission from American Chemical Society. (d) Schematic illustration of $Er^{3+}$ sensitized photon UC of a series of emitters ($A^{3+}$: $Nd^{3+}$, $Eu^{3+}$, $Ho^{3+}$, and $Tm^{3+}$) under 1532 nm excitation with modulation of $Yb^{3+}$. The dashed-blue, dashed-yellow, and solid arrows represent excitation, energy transfer, and emission processes, respectively [94]. Printed with permission from Wiley-VCH. (e) Schematic illustration of creating a set of UCNPs combining with NIR dyes with programmed excitation band wavelengths (ET: energy transfer) [95]. Printed with permission from Royal Society of Chemistry.



808 nm, which showed similar excitation efficiency but a greatly decreasing in tissue overheating effect when compared to that under 980 nm [88]. By rational design of the core/shell UCNPs, the UCL intensity was even lager when the energy back-transfer from emitters to $Nd^{3+}$ was eliminated [92]. This can be realized using UCNPs with a quenching-shield sandwich structure ($NaYF_4$:Yb/Er@$NaYF_4$:Yb@$NaNdF_4$:Yb) by optimizing the thickness of middle transition layer ($NaYF_4$:Yb), which bridges the energy transfer from $Nd^{3+}$ to emitter through $Yb^{3+}$ sublattice and, at the same time, acts as the shield to block the energy back-transfer from emitter to $Nd^{3+}$ (Fig. 5a). A similar work by Xie et al. has also demonstrated that doping $Nd^{3+}$ into a shell layer can efficiently suppress this energy-back transfer and facilitate the energy migration to a series of emitters ($Ho^{3+}$, $Tm^{3+}$, $Er^{3+}$) to give enhanced UCL, while keeping a high doping concentration of $Nd^{3+}$ at 20%. This enhanced UCL can be used for efficient bioimaging without auto-fluorescence and concern of overheating (Fig. 5b and c) [93]. More recently, a new sensitizer $Er^{3+}$, which transferred the absorbed energy (~1530 nm) at the second near-infrared biological window (1000–1700 nm) to the nearby emitters, has been reported in a brand new design of UCNPs (Fig. 5d) [94]. In this work, characteristic UCL emissions from the emitters ($Nd^{3+}$, $Eu^{3+}$, $Ho^{3+}$, and $Tm^{3+}$) were observed with $Er^{3+}$ codoped in $NaYF_4$ when excited at 1532 nm, revealing a versatile sensitizer of $Er^{3+}$. Enhancement of the UCL of the UCNPs can be performed by coating an inert shell ($NaYF_4$) or active shell ($NaYF_4$:Er). This availability of $Er^{3+}$ sensitized UCNPs showed great promise in anticounterfeiting based on orthogonal excitation.

In spite of the above advances, the choice of excitation wavelength for UNCPs is still very limited, which is one of the key roadblocks for further applications of UCNPs. Despite the inorganic shell via epitaxial growth, organic dyes can also be rationally designed to provide flexible excitation wavelengths. In a recent work, Xu et al. [95] reported a generic design to create a series of near-infrared dyes with systematically progressive absorption wavelengths (Fig. 5e). Through interacting with hydrophobic organic ligand free UCNPs, these antenna offered programmed excitation band wavelengths. In addition, mixed dyes can also be adopted to further provide expanded excitation bands of UCNPs. All the above results demonstrated that a core/shell structure could not only be harnessed to shift the excitation wavelength, but also maintain or enhance the UCL through doping the lanthanide ions spatially as well as integrate organic dyes, offering diversity and selectivity in the deep-tissue biological and anticounterfeiting applications.

### *Efficiency enhancement of emissions*

As discussed above, significant quenching effects arising from surface defects and surrounding ligands will cause extremely weak UCL intensity. This concern can also be addressed by employing one or multiple inert outer shells using epitaxial growth method. On one hand, this inert shell passivates the defects at the surface of the core nanoparticles and reduces the non-radiative energy transfer. On the other hand, it preserves the hooping energy in the core from dissipated in the surrounding solvents and ligands. In regard to this, several works have been performed utilizing inert shell to enhance the UCL intensities, including homogenous active core-inert shell structures ($NaYF_4$:Yb,Tm(Er)@$NaYF_4$ [29,96], $NaGdF_4$:Yb,Er@$NaYF_4$ [20], $NaYF_4$:Yb,Er(Tm)@$NaGdF_4$ [44,56], $NaGdF_4$:Yb,Er(Ho,Tm)@$NaGdF_4$ [97], $SrF_2$:Yb,Er@$SrF_2$ [98] and YOF:Yb,Er@YOF [99]), as well as heterogeneous active core-inert shells structures (β-$NaYbF_4$:Tm@$CaF_2$ [30] and α-$NaYF_4$:Yb,Er@$CaF_2$ [100]). In these active core/inert shell structures, the thickness of the shell plays a key role in enhancing the UCL intensity. For example, Zhang et al. [56] and Johnson et al. [34] demonstrated a linear dependence of both green and red UCL intensities when increasing the thickness of inert shell ($NaGdF_4$ or $NaYF_4$) on $NaYF_4$:Yb/Er core, which was due to the gradually weakening from the affection of surrounding quenchers (Fig. 6a). Later on, Li et al. introduced a flexible one pot successive SLBL

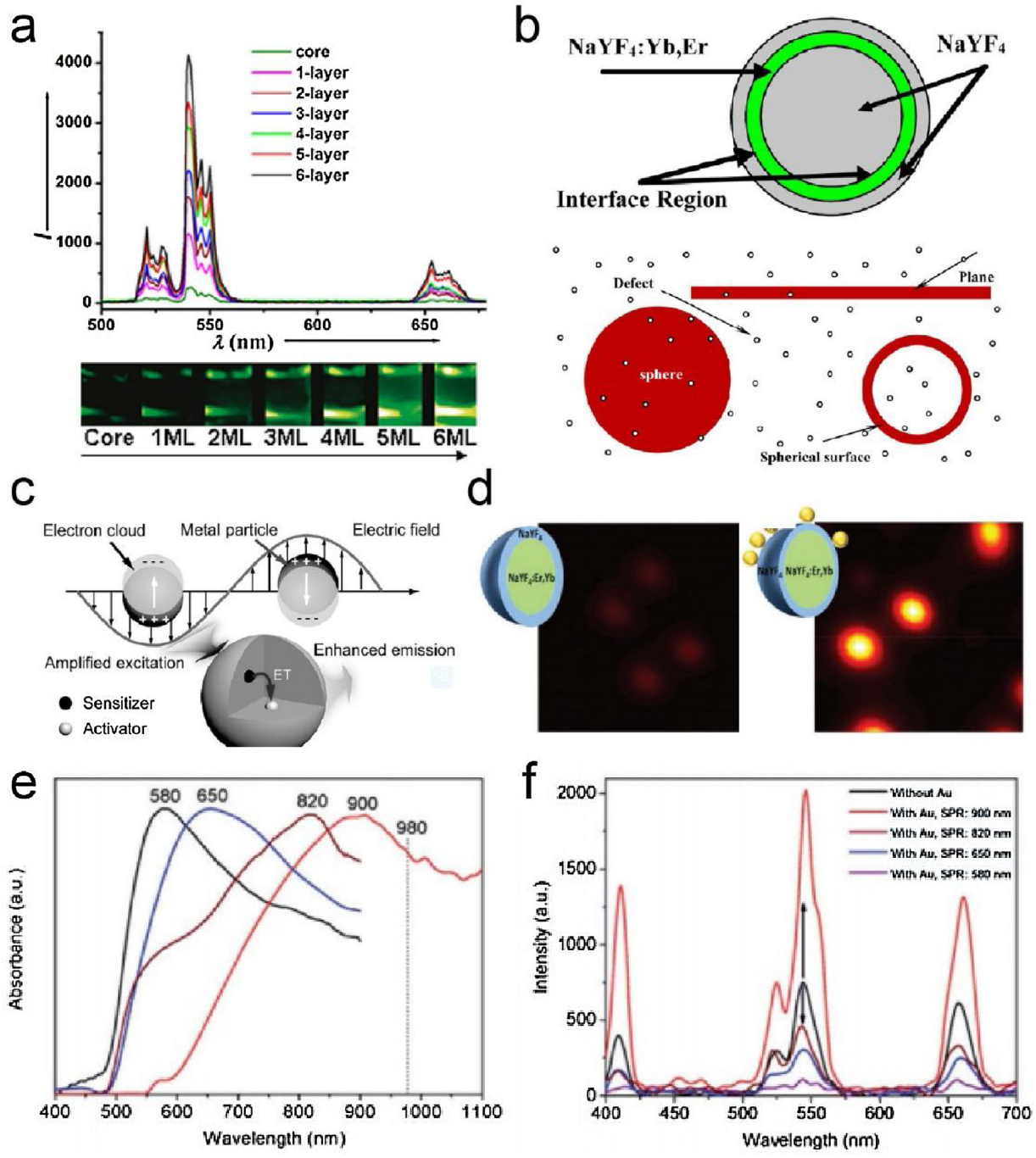


**Fig. 6.** (a) UCL spectra and photograph of $NaYF_4$:20%Yb/2%Er core nanocrystals and the corresponding core/shell nanocrystals with different monolayer (ML) of $NaGdF_4$ shell in cyclohexane solutions under excitation with 980 nm excitation [56]. Printed with permission from American Chemical Society. (b) top: schematic of an annular-doped $NaYF_4$:Yb/Er nanoparticles for δ-doped samples; bottom: schematic illustrations of the codoping spherical surface, plane, and sphere with a random distribution of defects throughout the samples [101]. Printed with permission from American Chemical Society. (c) Schematic illustration plasmonic enhancement of UCL [105]. Printed with permission from Wiley-VCH. (d) The scanning confocal images of the $NaYF_4$:Yb/Er@$NaYF_4$ and gold nanoparticles decorated $NaYF_4$:Yb/Er@$NaYF_4$ with 15 nm inert shell, demonstrating the plasmonic enhancement of UCL intensities [106]. Printed with permission from Royal Society of Chemistry. Absorption (e) and fluorescence (f) spectra of the gold-shell encapsulated $NaYF_4$:Yb/Er UCNPs with different surface plasmon resonance peaks [107]. Printed with permission from Royal Society of Chemistry.



strategy to synthesize the $NaGdF_4$:Yb,Er@$NaYF_4$ core/shell UCNPs [40]. A significant fluorescence enhancement as well as QY was obtained during the growth of the $NaYF_4$ shell, manifesting a QY 32 times higher than that of the bare core nanoparticles (~5 nm) when the thickness of shell reaches ~6 nm. These perspective results confirmed the effectiveness of a shell to suppress surface-related quenching effects.

In addition to the single inert shell, constructing UCNPs with multishell structures is also employed for enhancing the UCL intensity. Despite the successes in synthesizing high-quality UCNPs, defects emerge inevitably, not only on the surface but also randomly distributed in UCNPs. Therefore, the above way to coat inert shell on UCNP cores is not able to eliminate the inner defects (in 3D space). To solve this problem, a new δ-doping tech-

nique for boosting the emission efficiency of UCNPs was reported (Fig. 6b) [101]. In this protocol, a very thin and highly crystalline luminescent shell (<10 nm) was sandwiched between an inert core and an inert outer shell. Thus, the emitters in the luminescent shell are restricted to 2D plane, minimizing the interaction with randomly distributed inner defects and suppressing the energy transfer between lanthanide ions and defects. The δ-doping $NaYF_4$@$NaYF_4$:Yb/Er@$NaYF_4$ core/shell/shell nanoparticles enhanced both the green and red emission intensities when compared to the conventional $NaYF_4$:Yb/Er@$NaYF_4$ core/shell nanoparticles. In a similar work, Chen et al. also reported the δ-doping system composed of $NaYbF_4$:Tm to enhance muliphoton UC [102]. Efficient five-photon UC of $Tm^{3+}$ (emission at 290 nm) was demonstrated. They attributed this enhancement to the spatial confinement of energy migration in nanosized structure as well as inhibition of surface quenching effects.

Compared to the epitaxial growth of lanthanide doping shells above, nonepitaxial metallic shells are an alternative to increase the UCL intensity by coupling interested UCL with localized surface plasmon (LSP). When the frequency of incident light photons and the natural frequency of metallic nanostructures match, LSP resonance (LSPR) will occur and greatly enhance the electromagnetic field near the surface of the metallic nanoparticles [103,104]. This enhanced field, which falls off rapidly with the distance from the metallic surface, can induce an increase of emission efficiency of the near-by UCNPs by unambiguous amplifying the excitation flux and accelerating the radiative decay rate (Fig. 6c) [105]. Nevertheless, the distance between the surface of metal and the UCNPs determines the coupling effects, in which an optimized space is need to obtain the plasmonic enhancement of UCL emission [106]. Besides, the LSPR peak also has profound influence on the UCL intensity, which can be achieved by tuning the thickness of the coating metal [107]. By constructing core/shell UCNPs in an UCNPs@spacer@metal or metal@spacer@UCNPs configuration, large enhancement of UCL can be realized [106–109]. For example, Clarke et al. reported an easy and reliable method for the large-scale dewetting of plasmonic gold nanoparticles onto core/shell $NaYF_4$:Yb,Er@$NaYF_4$ UCNPs, in which the inert $NaYF_4$ shell was used to precisely tune the space between the UCNPs and the metal (Fig. 6d) [106]. Enhancement of UCL was demonstrated to be strongly dependent on the thickness of $NaYF_4$ shell, with a maximum enhancement factor of 5.5 in total emission intensity achieved by 10 nm $NaYF_4$ shell. To verify the effect of LSPR peaks on enhancing the UCL intensity, Priyam et al. reported a gold nanoshell encapsulation of silica coated $NaYF_4$:Yb/Er UCNPs using a poly-(amino acid) template and the intense LSPR peaks was tuned in a wide wavelength range from visible to NIR region (Fig. 6e) [107]. Due to the resonant between the absorption peak of UCNPs and the LSPR peak in NIR region, the UCL intensities of three emission peaks at 660 (red), 545 (green) and 410 nm (blue) can be enhanced by 2.1, 2.6 and 3.3 times, respectively (Fig. 6f).

Despite the above successes in enhancing the emission efficiency of UCNPs, their QY is still quite low, largely because of the comparatively low extinction coefficients of lanthanide ions and large surface to volume ratio with vast surface defects. This means that they hold great potential for an improvement in various applications. Therefore, consistent efforts are still needed to make to enhance the QY of UCNPs in addition to the above mentioned ways through constructing core/shell structure for enhancing excitation harvesting, surface passivation and LPS coupling.

*Multicolor modulation of emissions*

Multiplexing and displaying based on UCNPs present diverse advantages. Due to the unique 4f orbital structure, emissions from UCNPs are insensitive to the surroundings and narrower (full width at half maximum (FWHM) is ~10–20 nm) than that of QDs (FWHM is ~25–40 nm) and organic dyes (FWHM is ~30–100 nm), which enable a large number of identities. In addition to the enhancement of excitation and emission intensities, another promising characteristic of core/shell structure is to manipulate the optical emissions of UCNPs. In general, two main strategies are usually employed to achieve the purpose: a) through spatially isolated lanthanide ions directly; b) through the energy transfer methods.

Lanthanide elements are spectroscopically rich species and have a unique set of energy levels. Most of the lanthanide ions possess characteristic and distinguishable UCL. Among these ions, $Yb^{3+}$/$Er^{3+}$, $Yb^{3+}$/$Tm^{3+}$ and $Yb^{3+}$/$Ho^{3+}$ are the most commonly used luminescent pairs doped in fluoride host matrix with low phonon energy ($NaGdF_4$ or $NaYF_4$). In general, these pairs give green ($Er^{3+}$ and $Ho^{3+}$) and blue ($Tm^{3+}$) colors due to their main emission peaks attributed to $^2H_{11/2}$, $^4S_{3/2}\rightarrow{}^4I_{15/2}$ ($Er^{3+}$), $^5F_4\rightarrow{}^5I_8$ ($Ho^{3+}$) and $^1D_2\rightarrow{}^3F_4$, $^1G_4\rightarrow{}^3H_6$ ($Tm^{3+}$), respectively. It should be noted that different emission colors of UCNPs based on these emitters can be tuned by controlling the dopant concentrations or combination of different host/emitter [110–115]. However, the challenge of the former method is the deleterious cross relaxation due to high concentration of lanthanide dopants and the presence of multiple dopants, which could dramatically decrease the emission intensity. To address this issue, core/shell structure can be utilized by separating the emitters into different space, while maintaining their original colors with high emission efficiency. For example, Qian et al. reported hexagonal-phase core/shell $NaYF_4$:Yb/Tm@β-$NaYF_4$:Yb/Er and β-$NaYF_4$:Yb/Tm@β-$NaYF_4$:Yb/Er@β-$NaYF_4$:Yb/Tm nanoparticles, which can produce emissions from both $Er^{3+}$ and $Tm^{3+}$ when excited at 980 nm [116]. The displaying results were different from that of Tm/Er codoped $NaYF_4$ nanoparticles, whose fluorescence from $Tm^{3+}$ was quenched by the doped $Er^{3+}$. Moreover, by incorporating lanthanide ions with main emissions at blue, green and red region into a single nanostructure under sole light excitation, even a bright white light can be realized through the excitation power density induced multiphoton pathways regulation (Fig. 7a) [117]. In addition to the core/shell UCNPs exhibiting tunable UC emissions excited at the same wavelength, this structure also fulfils the separation of different lanthanide sensitizers spatially, leading to orthogonal emissions under different excitations. In these systems, $Nd^{3+}$ and $Yb^{3+}$ excited at ~800 and 980 nm are commonly used as combined sensitizers to activate each emission pathway. Attention should be paid that an inert layer or a absorption filtration shell must be introduced between these two sensitizers to make sure that only the $Nd^{3+}\rightarrow Yb^{3+}\rightarrow$emitter pathway can be activated under 808 nm excitation, which, in the meantime, are other blocked by the thick inert shell or absorbed by a filtration shell in the other emission pathway ($Yb^{3+}\rightarrow$emitters under 980 nm excitation) to preserve the pure excitation-emission properties from the separated emitters [60,118]. In addition, the distribution of the dopants confined in the core/shell can also be employed to regulate the emission colors, suggesting another facile route for development of novel UCL multiplexed probes. For example, our group synthesized a series of UCNPs with the same amount of $Er^{3+}$ dopants doped from outer shell to inner shell in consistent sized nanoparticles [40]. The according results showed that the ratio of red to green emissions was increased, leading to the change of emission color from green to yellowish green. The reason is attributed to the efficient cross relaxation processes among $Er^{3+}$ ions at high doping levels when the local relative concentration of dopants increased.

Through decently designed core/shell structures, the emissions of UCNPs can also be remotely controlled by only the excitation variations. In an exciting work, Deng et al. [119] reported a convenient and versatile method by adjusting the pulse width of the

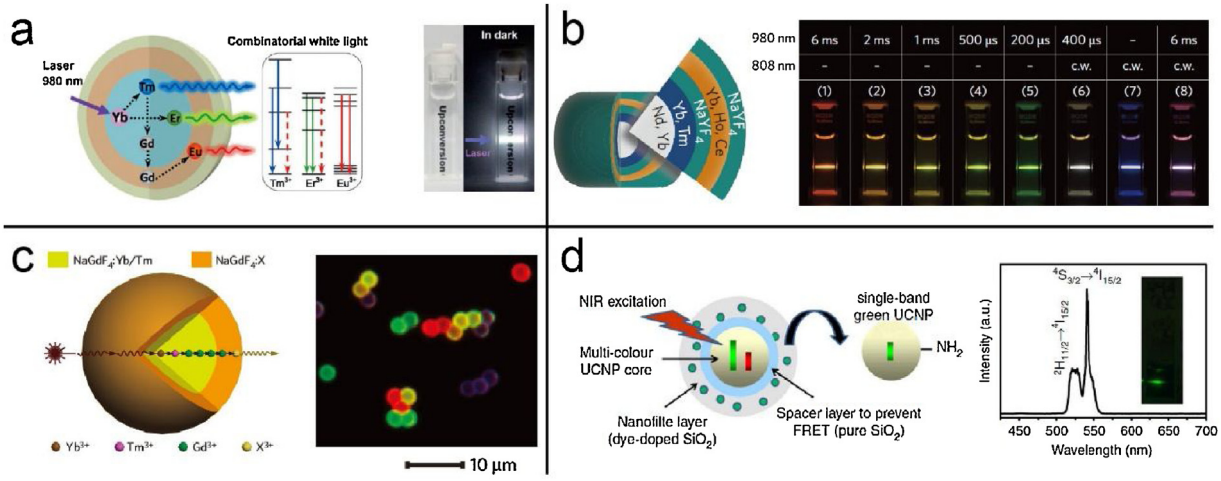


**Fig. 7.** (a) Schematic illustration of white-light-emitting nanostructure and simplified energy level diagram of blue, green, and red emissions (left); Photograph of white-light-emitting nanocrystals in daylight and under 980 nm excitation with a power density of 15 W $cm^{-2}$ (right) [117]. Printed with permission from Wiley-VCH. (b) Design of $NaYF_4$-based core/shell nanocrystals capable of emitting tunable colors when irradiated with NIR lasers (left); Luminescence photographs showing multi-color tuning (1–8) of the sample through combined use of 980 and 808 nm lasers (right) [119]. Printed with permission from Nature Publishing Group. (c) Schematic design of $NaGdF_4$:Yb/Tm@$NaGdF_4$ core/shell nanoparticles for energy migration UC (X: emitter ion) (left); Luminescence micrograph of polystyrene beads tagged with core/shell nanoparticles comprising $NaGdF_4$:Yb/Tm@$NaGdF_4$ (blue), $NaGdF_4$:Yb/Tm@$NaGdF_4$:Tb (green), $NaGdF_4$:Yb/Tm@$NaGdF_4$:Eu (red), and a binary mixture of $NaGdF_4$:Yb/Tm@$NaGdF_4$:Tb and $NaGdF_4$:Yb/Tm@$NaGdF_4$:Eu (yellow), respectively (right) [39]. Printed with permission from Nature Publishing Group. (d) Illustration diagram of green single band UCNPs fabrication (left) and its UCL spectra measured in water (right) [130]. Printed with permission from Nature Publishing Group.
Reproduced with permission. Copyright 2015, Wiley-VCH Verlag GmbH & Co. KGaA, Weinheim; Copyright 2011, 2015, Nature Publishing Group.

excitation light to dynamically tune the emissions of UCNPs in the full color range (Fig. 7b). This new class of core/multishell UCNPs were consisted of a $NaYF_4$ host matrix doped with $Tm^{3+}$ and $Ho^{3+}$ as the emitters in different shells. Under 808 nm excitation with a continuous wave, blue emission was obtained from $Tm^{3+}$. In addition, $Ho^{3+}$ was responsible for the red/green emissions under 980 nm. In their study, they found that deactivation of the excitation energy and energy transfer process occur at different rates. By codoping $Ce^{3+}$ with $Ho^{3+}$ in the same shell, different red/green emission intensity ratios were obtained by adjusting the pulse widths of 980 nm excitation, providing visible red emission or green emission. When combined the above three modes, different colors can be easily generated. Besides, excitation power also provides a convenient approach for modulating emission colors of UCNPs [120,121]. For example, excitation-power sensitive $NaYbF_4$:Ho nanoparticles were fabricated, which showed a large red-to-green emission intensity ratio from 0.37 to 5.19 by increasing the excitation power density [120]. This amplification of color tunability range was due to the maximal use of the incident energy enabled by concentrated $Yb^{3+}$. All these studies suggested the significance of the decently designed core/shell UCNPs in the emission color tunability.

As for other emitters lacking of ladder-like energy levels, such as $Sm^{3+}$, $Eu^{3+}$, $Tb^{3+}$ and $Dy^{3+}$, only simultaneous multiphoton absorption and cooperative sensitization upconversion can be adopted to achieve UC using NIR light [122–125]. The inherent limitation, however, is the requirement of either delicate and expensive pulsed laser or nonlinear optical materials. To realize tunable UC emissions of these emitters in a moderate and general way, a well-defined core/shell structure offers the possibility through $Gd^{3+}$ mediated energy migration (left in Fig. 7c) [39]. In this core/shell structure, $Tm^{3+}$ with much intense UC emissions in the UV range excited by $Yb^{3+}$ at ~980 nm is selectively doped and the high-lying excited energy can be transferred to the emitters through $Gd^{3+}$ sublattice. By introducing different emitters ($X^{3+}$ = $Sm^{3+}$, $Eu^{3+}$, $Tb^{3+}$ and $Dy^{3+}$) in the structure, colorful emissions of the particles can be regulated (right in Fig. 7c). Similarly, a protective outer inert shell enables to effectively suppress the surface-related quenching effects [126]. This control of energy migration opens a new realm for exploiting the optical properties of widely lanthanide ions.

Apart from the lanthanide dopants distributed in a confined nanoscale region, the nonradiative energy transfer also provides a direct means to manipulate the property of UCL. When the UCNPs are used as energy donor and organic dyes or QDs are served as energy acceptors, nonradiative energy may transfer via multipolar interaction, which essentially changes the energy distribution in certain energy levels of UCNPs, leading to alteration of the UC emission wavelengths with a large freedom [127–129]. The effect of this interaction shows strongly dependent on the distance of ions. Based on this strategy, an example was provided by Li et al. who synthesized hexagonal-phase $NaYF_4$:Yb/Er(Tm) nanoparticle as the core with very thin and uniform silica shell encapsulating tetramethylrhodamine isothiocyanate (TRITC) or QDs (QD605) [129]. The original blue (emission from $Tm^{3+}$) and yellow green (emission from $Er^{3+}$) emissions from the UCNPs were altered to orange and red color due to the combination with downconversion emissions from TRITC and QDs, respectively, after absorption of the visible fluorescence from their UNCP cores. Cheng et al. also adopted this strategy by loading fluorescence and quenching molecules in amphiphilic polymer functionalized UCNPs [128]. As many as five tuned visible emission colors were obtained from these UCNP-dye complexes and used for in vivo multicolor imaging. Alternatively, the emission light from the UCNP donors can also be absorbed by the acceptor molecules, resulting in missing of some spectra located in the absorption region of the acceptor and in changing of final colors. Our group has reported single-band emission UCNPs utilizing organic dyes as filters (Fig. 7d) [130]. In these systems, nickel (II) phthalocyanine-tetrasulfonic acid tetrasodium salt (NPTAT) (maximum absorption wavelength at 657 nm) or rhodamine B isothiocyanate (maximum absorption wavelength at 555 nm), loaded into the outer silica shell of UCNPs, were chosen to eliminate the extra red or green emission band of three types

of UCNPs, respectively. The obtained blue-, green- and red single-band UC nanoprobes were successfully applied to determine the expression levels of three biomarkers in both human breast cancer cells and paraffin-embedded clinical tissue sections, showing a promising prospect for next-generation applications in the life sciences.

*Luminescence lifetime modulation*

Trivalent lanthanide ions usually exhibit longer lifetime from microseconds (e.g. $Yb^{3+}$, $Nd^{3+}$) to even milliseconds (eg. $Eu^{3+}$, $Tb^{3+}$). Compared to fluorescence intensity-based imaging, fluorescence lifetime shows an improved sensitivity when time-gated detection method is used to remove the autofluorescence background (lifetime at nanosecond range) (Fig. 8a) and provides reproducible quantitative measurements over time due to its less dependent on the materials concentration [131–133]. In addition, the lifetime values can constitute a new temporal dimension for expanding the optical codes in various applications.

The most common ways for tuning the lifetime of UCNPs are based on altering the concentration of dopants and the size of UCNPs [134,135]. When the concentration of dopants increases, lifetime of the UCNPs decreases continually due to the cross relaxation effects. As for the size tunability, smaller UCNPs retain a higher density of volume defects due to the larger surface to volume ratio, which accelerates the radiative process and leads to lower lifetimes. Accordingly, core/shell structures can be realized to modulate the lifetimes by suppressing the above deleterious energy dissipation processes, thereby increasing the lifetime. For example, Wang et al. fabricated a series of $NaYF_4$:Yb/Er@$NaYF_4$ core/shell nanoparticles. When the shell thickness increased from 0 to 2.8 nm, lifetimes of emission at 540 nm from $Er^{3+}$ elevated from 88 to 301 μs [135]. One the other hand, when active shell ($NaYF_4$:Yb) was coated with a consistent thickness (~1.8 nm), the lifetimes showed an reverse correlation (decreasing from 231 μs to 138 μs) with increasing the concentration of $Yb^{3+}$ from 0 to 20% [135]. These results suggested that combining with different energy distributors (e.g. surface defects, dopants) can precisely deplete the excited states of $Yb^{3+}$, thus allowing to control the emission lifetime in a facile way within a wide range. In addition to coating the outer shell to modulate the hooping energy, the spatial distribution of the dopants can also impact the lifetime of UCNPs. Chen et al. found that $Yb^{3+}$ and $Er^{3+}$ distributed in a two-dimensional thin layer as in the δ-doping configuration resulted in declined lifetimes of $Er^{3+}$ emissions at 540 and 654 nm under both 808 and 980 nm excitations, respectively, as compared to the distribution of these ions in a three-dimensional sphere [136]. The reason of reduced lifetime could be attributed to the short distance between the adjacent ions in the two-dimension thin layer, which was beneficial to induce efficient cross-relaxations. Very recently, our group has reported a new strategy to manipulate the fluorescence lifetime of UCNPs for high capacity multiplexed biodetection [137]. The rationally designed core/shell structure for lifetime tunability consisted of, from inner to outer side, a luminescent core, an energy relay shell, an energy absorption shell and an outer inert shell (Fig. 8b). When increasing the thickness of the middle energy relay shell, the diffusive energy migration process in this shell prolongs the average waiting time (the effective lifetime) for energy of a relay ion in the absorption layer to migrate to emitters in the luminescent core, which is proportional to the shell thickness. In this work, single blue emission β-$NaGdF_4$:Yb/Tm@$NaYF_4$:Yb@$NaNdF_4$:Yb@$NaYF_4$ UCNPs were fabricated. When the thickness of $NaYF_4$:Yb adjusted from 1.5 to 5.4 nm, lifetime at the blue emission band (475 nm) increased from 632 to 836 μs (left in Fig. 8c). The same trend of lifetimes were also presented in single green (550 nm) and red (660 nm) emission UCNPs (middle and right in Fig. 8c). This lifetime tunability combined with emission wavelengths enabled the multiplexed detection of human papilloma virus (HPV) subtypes in patient samples and robust anti-counterfeiting. In addition to the UC process, the energy relay approach also showed an effective tunability of lifetime on the downconverting way, which spanned three orders of magnitude with a single emission band (Fig. 8d) [138].

*Modulation of functional multiplicity*

Despite of exploiting the above optical properties of UCNPs for bioimaging, the core/shell structure is also feasible to provide a straightforward platform for multi-functionality, including incorporating new imaging modalities and therapeutic functions, which can expand applications of UCNPs for biomedical and life sciences, without interference in between to provide precise and comprehensive analysis of disease.

These new imaging modalities are mainly from special elements: for example, magnetic elements (such as $Gd^{3+}$, $Mn^{2+}$, $Dy^{3+}$ and $Ho^{3+}$) allow magnetic resonance imaging (MRI), high X-ray attenuation elements (such as $Lu^{3+}$, $Yb^{3+}$) offer computed tomography (CT) imaging, while $^{18}F$ and $^{153}Sm$ radionuclide are responsible for positron emission tomography (PET) and single-photon emission computed tomography (SPECT) imaging, respectively. By appropriately tailoring the structure of UCNPs and rationally introducing these elements into the core as well as the shell, a dual bioimaging system, such as UCL/MRI [139–141], UCL/CT [142–144] and ULC/PET [145], or a multimode bioimaging system, such as trimodal ULC/MRI/CT [83,146–148] as well as four modal UCL/CT/MR/SPECT [65] can be successfully constructed. For example, Li et al. designed a core/shell/shell nanocomposite $NaYbF_4$:Tm@$CaF_2$@$NaDyF_4$ for tri-modal bioimaging [147]. First, under 980 nm excitation, intense NIR UC emission from $Tm^{3+}$ at 800 nm was used for in vivo small animal imaging with a high signal to noise ratio (~32) in lymphatic node. Then, the heavy atoms Yb and Dy can be adopted as a high X-ray mass absorber. A high CT value of 490 HU indicating the potential of the nanocomposite as an efficient CT imaging contrast agent. Moreover, the introduction of $Dy^{3+}$ based host as an outer shell also displayed an excellent r2 relaxivity in MRI imaging (41.1 $mM^{-1}s^{-1}$). It can be definite that the multi-mode bioimaging system could realize increasingly precise localization and detection of disease with complementary advantages. Although promising, it is challenge to maintain each of the bioimaging modalities at the optimized condition when integrating different composites into a single UCNP. To address this issue, He et al. reported heteroepitaxial core/shell/shell β-$NaYb/ErF_4$@$NaLuF_4$@$NaGdF_4$ UCNPs as a UCL, CT and MRI imaging contrast agent, which showed concurrently enhanced performance compared to their individual imaging components when increasing the thickness of the $NaLuF_4$ interfacial layer (Fig. 9a and b) [146]. The reason is that the thicker NaLuF4 layer a) allows heavy atoms ($Lu^{3+}$) to attenuate more X-rays for enhanced CT contrast; b) acts as a thick epitaxial shell that shields $Yb^{3+}$/$Er^{3+}$ luminescent centers in the core from surface quenching, thereby enhancing the UCL; c) acts as a larger substrate to decelerate the tumbling of all paramagnetic $Gd^{3+}$ centers in the $NaGdF_4$ thin layer, thus enhancing the MRI.

In addition to the new bioimaging modalities, therapeutic functions can also be introduced through the delicate core/shell structure. In general, this is usually realized by coating an outer silica shell onto the core or core/shell UCNPs due to their lack of therapeutic effect. The silica shell has a well-developed surface chemistry and can be well-controlled in porosity for loading and controlled releasing payloads [49,50,59,148,149]. Liu et al. presented a specific mesoporous silica-coated $NaYF_4$:Yb/Tm@$NaYF_4$ UCNPs as an anticancer drug release system triggered by NIR light [49]. Azobenzene (azo) as well as the anticancer drug DOX were

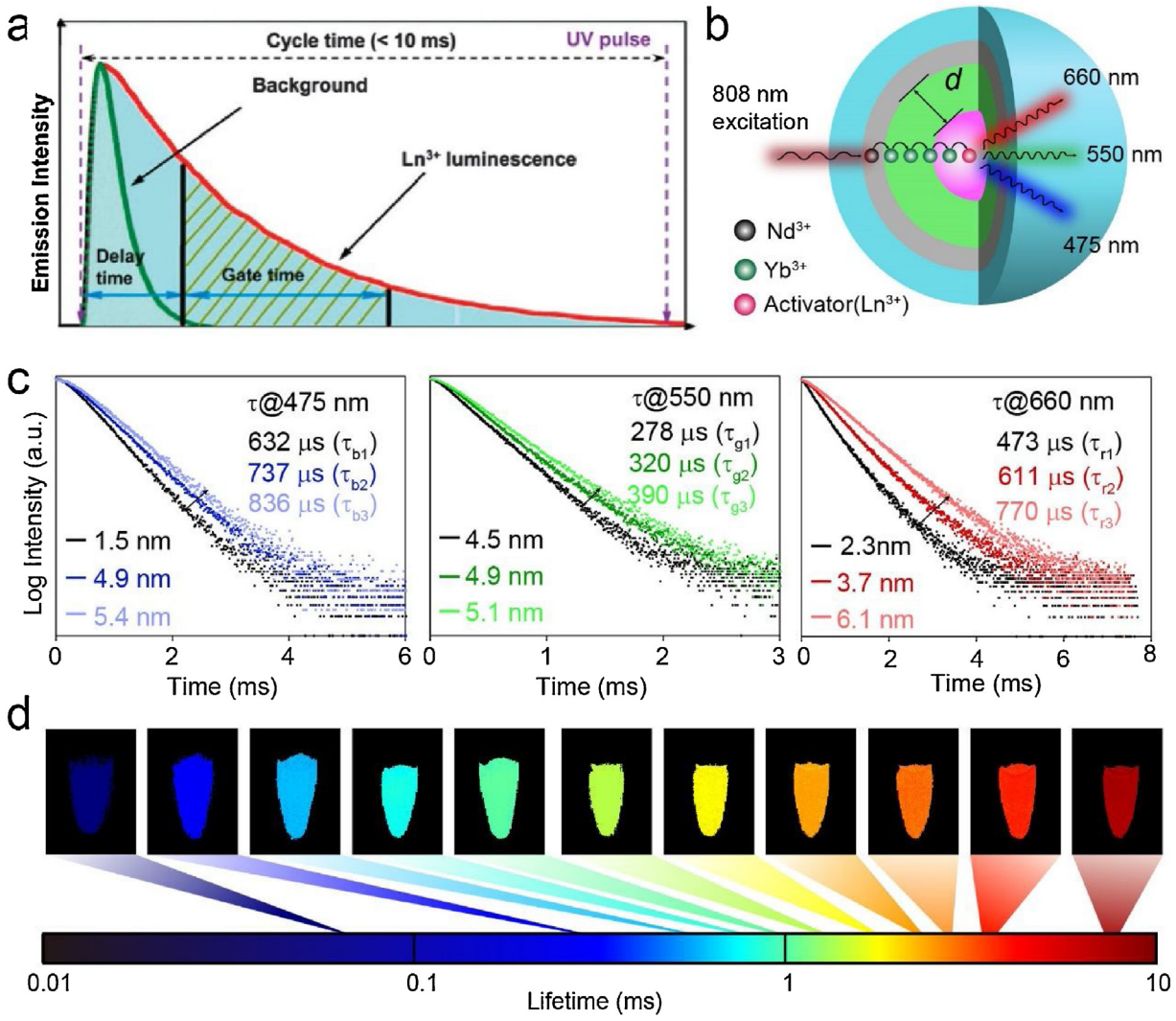


**Fig. 8.** (a) The principle of time-gated biosensing based on the long-lived UCL [133]. Printed with permission from Royal Society of Chemistry. (b) Schematic design of the $NaGdF_4$@$NaYF_4$@$NaNdF_4$@$NaYF_4$ core/shell/shell/shell nanoparticles for blue, green and red UCL [137]. Printed with permission from Wiley-VCH. (c) Decay curves of blue (475 nm), green (550 nm) and red (660 nm) emissions of the core/shell/shell/shell nanoparticles in (b) with increased thickness of energy relay layer under 808 nm excitation [137]. Printed with permission from Wiley-VCH. (d) Pseudocolor-mapped lifetime images of the $NaGdF_4$@$NaGdF_4$:Yb/Er@$NaYF_4$:Yb@$NaNdF_4$:Yb nanoparticles contained in centrifuge tubes [138]. Printed with permission from Nature Publishing Group.



loaded into the silica mesopores. Upon NIR laser irradiation, the azo molecules can act as a "stirrer" due to their reversible trans–cis photoisomerization in the mesopores under the upconverted UV (350 nm) and visible (450 nm) light emissions from the UCNPs simultaneously, creating a continuous rotation-inversion movement to trigger the release of the DOX. The amount of the in vivo drug release can be well controlled by varying the intensity and time duration of NIR exposure. To track the drug delivery system and monitor the drug-release percentage in vivo, our group has reported a novel absorption competition-induced emission (ACIE) system using $Nd^{3+}$-based mesoporous microcarrier and NPTAT organic dyes (Fig. 9c) [59]. A pH activated succinylated soy protein isolate polymer (SSPI) was used to seal the payload of protein-NPTAT complexes into the silica mesopores. $Nd^{3+}$ of the microcarrier can be excited under both 730 and 808 nm light to give NIR light at 1060 nm. While the former emission pathway can be efficiently blocked due to absorption competition between NPTAT, which showed ~2000-fold higher absorption coefficient, and $Nd^{3+}$ at 730 nm, the lateral was barely affected due to minimal absorption of NPTAT at 808 nm. The microcarrier stayed stable in acid environment (stomach and duodenum) and sustained release of the drugs happened in the alkaline environment of intestine due to the deprotonation of the SSPI on the outer surface of the microcarrier. Therefore, the recovered NIR light under 730 nm excitation can monitor the drug release and the stable NIR light under 808 nm can track the fate of the microcarriers and as a reference to estimate the release percentage in real time.

## Conclusions and outlooks

In this review, we surveyed and summarized recent progress in fabrication, characterization and optical properties tunability of core/shell UCNPs. Due to the intrinsic nature of 4f-4f optical transitions in lanthanide ions induced low extinction coefficient, the

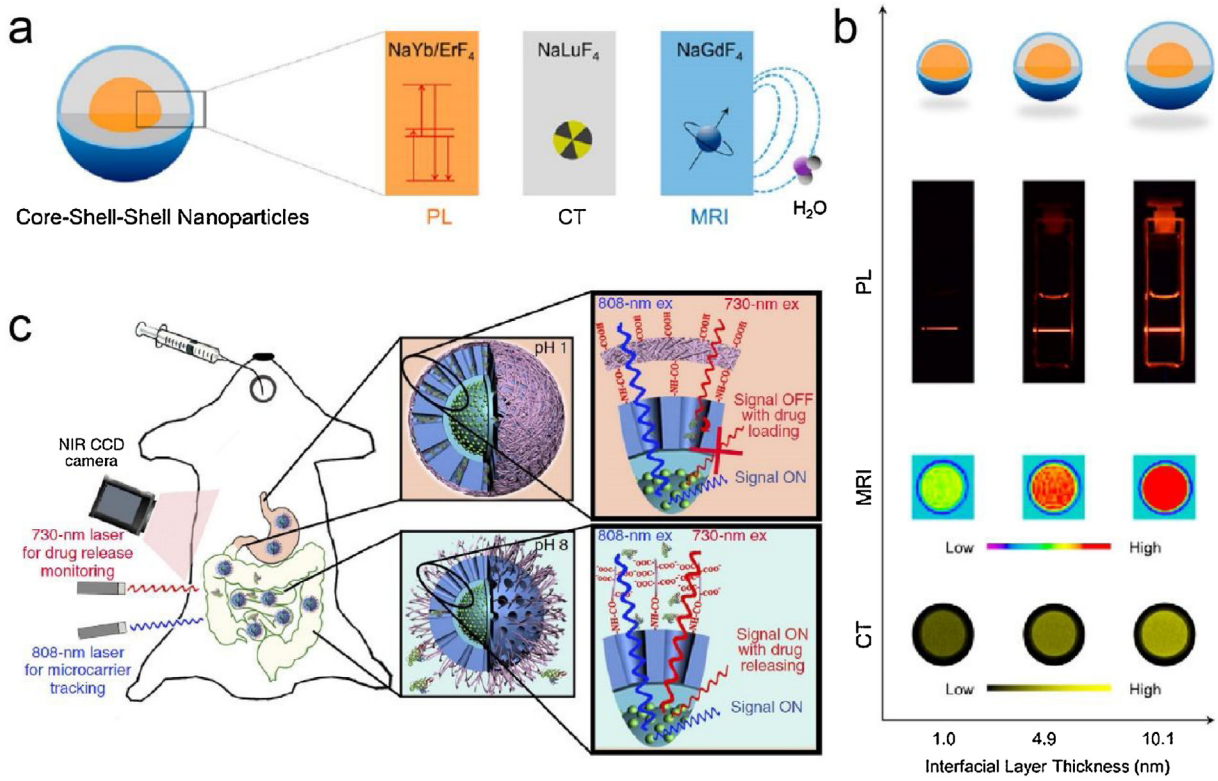


**Fig. 9.** (a) Schematic illustration for the β-NaYb/$ErF_4$@$NaLuF_4$@$NaGdF_4$ heteroepitaxial core/shell/shell NPs and their use for three modality imaging: PL, MRI and CT [146]. Printed with permission from American Chemical Society. (b) Cuvette images, MRI phantom images, and CT phantom images of the β-NaYb/$ErF_4$@$NaLuF_4$@$NaGdF_4$ CSS NPs with increased thickness of the interfacial $NaLuF_4$ layer, demonstrating the concurrently enhanced performance of the facile designed nanoparticles [146]. Printed with permission from American Chemical Society. (c) Schematic illustration of the absorption competition-induced emission bioimaging system [59]. Printed with permission from Nature Publishing Group.



luminescence efficiency of UCNPs is not comparable to semiconductor nanocrystals (QDs) or organic dyes, especially for ultra-small nanoparticles (<10 nm) with high surface to volume ratio. The introduction of a rationally designed protection shell coating on the UC core provides an effective way to suppress the surface-related quenching effects and enhance the light harvesting, leading to the improvement of UC performance. Besides, the structure enables to easily manipulate the ion-to-ion distance and spatial arrangement of different dopants, offering a facile strategy to tune the emission color as well as lifetimes of UCNPs for optical multiplexing, security, anti-counterfeiting and background-less bioimaging. More importantly, constructing from metal and organic dyes and QDs as the optical components renders highly flexible in core/shell nanoparticle design, in parallel with additional new functionalities for a wide range of applications.

Although much efforts for designing and biological applications of core/shell UCNPs have been made, numerous challenges still exist regarding to the real usage of core/shell UNCPs in near future. The first challenge is expanding the excitation and emission wavelengths of UCNPs. Lanthanide ions have abundant energy levels, but most of the corresponding spectra have not been realized and studied. Until now, only a few lanthanide ions are commonly used with limited emissions (e.g. $Er^{3+}$ with green/red emissions, $Ho^{3+}$ with green/red emissions and $Tm^{3+}$ with blue emission) and excitation wavelengths (e.g. $Nd^{3+}$ at 808 nm, and $Yb^{3+}$ at 980 nm). Therefore, exploiting UCNPs with tunable emissions or single wavelength emission as well as broadening the excitation wavelengths may hold promise in a wide range of applications. The second challenge is the low UCL intensity of UCNPs. Constructing core/shell structure may boost the luminescence of UCNPs compared to the core only nanoparticles, however, the QY is still much lower than their bulk counterparts, especially for the increasing researches on in vivo bioapplications using laser power density lower than the threshold ($\tilde{7}30$ mW/$cm^2$ and $\tilde{3}29$ mW/$cm^2$ for the common 980 and 808 nm laser respectively). Due to the strong dependence on the excitation density, significant lower UCNPs QY is obtained at low irradiance at $\tilde{0}.1$ W/$cm^2$. Therefore, developing advanced strategies to further enhance the brightness of core/shell UCNPs are essential. For example, emerging strategies are host lattice manipulation and photonic crystal engineering. The third challenge is to synthesis ultra-small (<10 nm) UCNPs with high brightness. UCNPs are not biodegradable, the accumulation of UCNPs for a long time in organs may cause severe side-effect. It has been shown that ultra-small nanoparticles can be rapid cleared from the renal routes to eliminate the cytotoxicity issue for future clinical use. Therefore, bright and ultra-small UCNPs may show enormous potential as bioimaging probes. Adopting shells or coupling with noble metal can efficiently enhance the brightness of UCNPs, however, the size of which will also synchronously increase. Therefore, it is highly desired to find new ways to solve this contradictory problems. A recent study has reported a simple and reproducible approach to successfully synthesize ultra-small core/shell UCNPs ($\tilde{5}$–6 nm) with up to $\tilde{1}000$ fold enhanced UCL intensity compared to the core nanoparticles, which may hold promise for high contrast bioimaging and rapid renal clearance from the body [97]. The forth challenge is the concentration quenching effects, which are ubiquitous in UCNPs due to

their intrafiguraltional properties. In contrast to QDs, UCNPs contain individual absorption and emission centers (lanthanide ions), which means that the UCL brightness can be apparently boosted through directly increasing the concentrations of dopants. However, due to the energy loss resulted from cross-relaxation, the concentration quenching constrained the heavily doped UCNPs (emitters are usually kept <2%) and their luminescence properties for further use. Although nanoparticles with core/shell structure can amend the concentration quenching effects to some extent by separating the highly doped dopants spatially and precisely control the energy migration process, there is still ample room for further luminescence improvement. Therefore, the delicate nanostructure design to completely eliminate the concentration quenching effects may fully open doors for many ground-breaking UC applications. The fifth challenge is the light harvesting ability of core/shell UCNPs. Due to the intrinsic nature, the absorption bands for the lanthanide ions are extremely narrow and low. Although a set of lanthanide ions can be incorporated into the core and shells to simultaneously harvest the specific NIR light, this limited light harvesting ability based only on lanthanide ions may still limit the UCNPs brightness for bioapplications as well as use in solar cells. In future studies, nonepitaxially combining more organic dye or noble metal antenna with broad absorption from UV to NIR may show promise in further boosting the UCL intensities of core/shell UCNPs. The sixth challenge is the issue of reproducibility and scalability of UCNPs. Up to now, almost all the UCNPs are limited to be synthesized in laboratory based on the fabrication approaches mentioned above and the size and optical performance of this available lab-scale products may vary from batch to batch, which inevitably hinders their practical bioapplications. Therefore, establishing a general approach for the large-scale synthesis of UCNPs is urgent. For example, You et al. developed a facile solid-liquid-thermal-decomposition (SLTD) method and applied in the scale-up synthesis of core/shell β-NaGdF4:Yb/Er@NaYF4 nanoparticles (up to 63 g) with narrow size variation (<7%) [150]. Last but not least, the seventh challenge is the standard measurement facilities and protocols for UCNPs. In comparison with imaging probes such as QDs and organic dyes, which are compatible with commercial fluorescence instrumentation, most of the detection equipments for optical characterization of UCNPs are home-made. Therefore, UCNPs with identical compositions synthesized with different methods in different groups may appear varied optical performance. It is highly desired to establish a standard evaluation criterion in both synthetic approaches and the measurement facilities. Additionally, multimodal imaging probes and detection systems should be paid increase attention in the future.

## Acknowledgements

The work was supported by the National Key R & D Program of China (2017YFA0207303), National Science Fund for Distinguished Young Scholars (21725502), Key Basic Research Program of Science and Technology Commission of Shanghai Municipality (17JC1400100).

## References

[1] G. Chen, H. Qiu, P.N. Prasad, X. Chen, Chem. Rev. 114 (2014) 5161–5214.
[2] M. Haase, H. Schafer, Angew. Chem. 50 (2011) 5808–5829.
[3] X. Li, F. Zhang, D. Zhao, Chem. Soc. Rev. 44 (2015) 1346–1378.
[4] L. Liang, Y. Liu, C. Bu, K. Guo, W. Sun, N. Huang, T. Peng, B. Sebo, M. Pan, W. Liu, S. Guo, X.Z. Zhao, Adv. Mater. 25 (2013) 2174–2180.
[5] Y. Liu, Y. Lu, X. Yang, X. Zheng, S. Wen, F. Wang, X. Vidal, J. Zhao, D. Liu, Z. Zhou, C. Ma, J. Zhou, J.A. Piper, P. Xi, D. Jin, Nature 543 (2017) 229–233.
[6] L. Prodi, E. Rampazzo, F. Rastrelli, A. Speghini, N. Zaccheroni, Chem. Soc. Rev. 44 (2015) 4922–4952.
[7] Y. Liu, K. Ai, L. Lu, Nanoscale 3 (2011) 4804–4810.
[8] L. Wang, P. Li, Y. Li, Adv. Mater. 19 (2007) 3304–3307.
[9] Z.-L. Wang, J.H. Hao, H.L.W. Chan, J. Mater. Chem. 20 (2010) 3178.
[10] P.A. Franken, A.E. Hill, C.W. Peters, G. Weinreich, Phys. Rev. Lett. 7 (1961) 118–119.
[11] N. Morishige, W.M. Petroll, T. Nishida, M.C. Kenney, J.V. Jester, J. Cataract Refract. Surg. 32 (2006) 1784–1791.
[12] P. Pantazis, J. Maloney, D. Wu, S.E. Fraser, Proc. Natl. Acad. Sci. U. S. A. 107 (2010) 14535–14540.
[13] W. Kaiser, C.G.B. Garrett, Phys. Rev. Lett. 7 (1961) 229–231.
[14] D.R. Larson, W.R. Zipfel, R.M. Williams, S.W. Clarke, M.P. Bruchez, F.W. Wise, W.W. Webb, Science 300 (2003) 1434–1436.
[15] A. Picot, A. D'Aleo, P.L. Baldeck, A. Grichine, A. Duperray, C. Andraud, O. Maury, J. Am. Chem. Soc. 130 (2008) 1532–1533.
[16] A.P. Alivisatos, Science 127 (1996) 933–937.
[17] A.R. Armstrong, P.G. Bruce, Nature 381 (1996) 466–500.
[18] W.C. Chan, S.M. Nie, Science 281 (1998) 2016–2018.
[19] F. Wang, J. Wang, X. Liu, Angew. Chem. 49 (2010) 7456–7460.
[20] C. Wurth, S. Fischer, B. Grauel, A.P. Alivisatos, U. Resch-Genger, J. Am. Chem. Soc. 140 (2018) 4922–4928.
[21] K. Kompe, H. Borchert, J. Storz, A. Lobo, S. Adam, T. Moller, M. Haase, Angew. Chem. 42 (2003) 5513–5516.
[22] X.G. Peng, M.C. Schlamp, A.V. Kadavanich, A.P. Alivisatos, J. Am. Chem. Soc. 119 (1997) 7019–7029.
[23] D.V. Talapin, A.L. Rogach, A. Kornowski, M. Haase, H. Weller, Nano Lett. 1 (2001) 207–211.
[24] S. Gai, C. Li, P. Yang, J. Lin, Chem. Rev. 114 (2014) 2343–2389.
[25] L. Sun, R. Wei, J. Feng, H. Zhang, Coord. Chem. Rev. 364 (2018) 10–32.
[26] G. Chen, H. Agren, T.Y. Ohulchanskyy, P.N. Prasad, Chem. Soc. Rev. 44 (2015) 1680–1713.
[27] X. Chen, D. Peng, Q. Ju, F. Wang, Chem. Soc. Rev. 44 (2015) 1318–1330.
[28] M.M. Lezhnina, T. Jüstel, H. Kätker, D.U. Wiechert, U.H. Kynast, Adv. Funct. Mater. 16 (2006) 935–942.
[29] G.-S. Yi, G.-M. Chow, Chem. Mater. 19 (2007) 341–343.
[30] G. Chen, J. Shen, T.Y. Ohulchanskyy, N.J. Patel, A. Kutikov, Z. Li, J. Song, R.K. Pandey, H. Ågren, P.N. Prasad, G. Han, ACS Nano 6 (2012) 8280–8287.
[31] F. Vetrone, R. Naccache, V. Mahalingam, C.G. Morgan, J.A. Capobianco, Adv. Funct. Mater. 19 (2009) 2924–2929.
[32] P. Huang, W. Zheng, S. Zhou, D. Tu, Z. Chen, H. Zhu, R. Li, E. Ma, M. Huang, X. Chen, Angew. Chem. 53 (2014) 1252–1257.
[33] F. Wang, R. Deng, X. Liu, Nat. Protoc. 9 (2014) 1634–1644.
[34] N.J. Johnson, A. Korinek, C. Dong, F.C. van Veggel, J. Am. Chem. Soc. 134 (2012) 11068–11071.
[35] S. Dühnen, M. Haase, Chem. Mater. 27 (2015) 8375–8386.
[36] K.A. Abel, J.C. Boyer, F.C. van Veggel, J. Am. Chem. Soc. 131 (2009) 14644–14645.
[37] K.A. Abel, J.-C. Boyer, C.M. Andrei, F.C.J.M. van Veggel, J. Phys. Chem. Lett. 2 (2011) 185–189.
[38] F. Zhang, R. Che, X. Li, C. Yao, J. Yang, D. Shen, P. Hu, W. Li, D. Zhao, Nano Lett. 12 (2012) 2852–2858.
[39] F. Wang, R. Deng, J. Wang, Q. Wang, Y. Han, H. Zhu, X. Chen, X. Liu, Nat. Mater. 10 (2011) 968–973.
[40] X. Li, D. Shen, J. Yang, C. Yao, R. Che, F. Zhang, D. Zhao, Chem. Mater. 25 (2012) 106–112.
[41] S. Fischer, J.K. Swabeck, A.P. Alivisatos, J. Am. Chem. Soc. 139 (2017) 12325–12332.
[42] B. Chen, F. Wang, Nanoscale 10 (2018) 19898–19905.
[43] C. Dong, F.C.J.M. van Veggel, ACS Nano 3 (2008) 123–130.
[44] C. Dong, A. Korinek, B. Blasiak, B. Tomanek, F.C.J.M. van Veggel, Chem. Mater. 24 (2012) 1297–1305.
[45] S. Han, X. Qin, Z. An, Y. Zhu, L. Liang, Y. Han, W. Huang, X. Liu, Nat. Commun. 7 (2016) 13059.
[46] H. Zhang, Y. Li, I.A. Ivanov, Y. Qu, Y. Huang, X. Duan, Angew. Chem. 49 (2010) 2865–2868.
[47] C. Yan, A. Dadvand, F. Rosei, D.F. Perepichka, J. Am. Chem. Soc. 132 (2010) 8868–8869.
[48] J.V. Garcia, J. Yang, D. Shen, C. Yao, X. Li, R. Wang, G.D. Stucky, D. Zhao, P.C. Ford, F. Zhang, Small 8 (2012) 3800–3805.
[49] J. Liu, W. Bu, L. Pan, J. Shi, Angew. Chem. 52 (2013) 4375–4379.
[50] X. Li, L. Zhou, Y. Wei, A.M. El-Toni, F. Zhang, D. Zhao, J. Am. Chem. Soc. 136 (2014) 15086–15092.
[51] R. Deng, X. Xie, M. Vendrell, Y.T. Chang, X. Liu, J. Am. Chem. Soc. 133 (2011) 20168–20171.
[52] M.K. Gnanasammandhan, N.M. Idris, A. Bansal, K. Huang, Y. Zhang, Nat. Protoc. 11 (2016) 688–713.
[53] Z. Luo, L. Zhang, R. Zeng, L. Su, D. Tang, Anal. Chem. 90 (2018) 9568–9575.
[54] D. Wang, R. Wang, L. Liu, Y. Qu, G. Wang, Y. Li, Sci. China Mater. 60 (2016) 68–74.
[55] L. Zeng, L. Xiang, W. Ren, J. Zheng, T. Li, B. Chen, J. Zhang, C. Mao, A. Li, A. Wu, RSC Adv. 3 (2013) 13915.
[56] F. Zhang, G.B. Braun, A. Pallaoro, Y. Zhang, Y. Shi, D. Cui, M. Moskovits, D. Zhao, G.D. Stucky, Nano Lett. 12 (2012) 61–67.
[57] Y. Zhang, Z. Hong, Nanoscale 5 (2013) 8930–8933.
[58] L. Zhou, X. Zheng, Z. Gu, W. Yin, X. Zhang, L. Ruan, Y. Yang, Z. Hu, Y. Zhao, Biomaterials 35 (2014) 7666–7678.
[59] R. Wang, L. Zhou, W. Wang, X. Li, F. Zhang, Nat. Commun. 8 (2017) 14702.
[60] X. Li, Z. Guo, T. Zhao, Y. Lu, L. Zhou, D. Zhao, F. Zhang, Angew. Chem. 55 (2016) 2464–2469.

[61] R. Wang, X. Li, L. Zhou, F. Zhang, Angew. Chem. 53 (2014) 12086–12090.
[62] N.J. Johnson, S. He, S. Diao, E.M. Chan, H. Dai, A. Almutairi, J. Am. Chem. Soc. 139 (2017) 3275–3282.
[63] J. Zuo, D. Sun, L. Tu, Y. Wu, Y. Cao, B. Xue, Y. Zhang, Y. Chang, X. Liu, X. Kong, W.J. Buma, E.J. Meijer, H. Zhang, Angew. Chem. 57 (2018) 3054–3058.
[64] B. Chen, D. Peng, X. Chen, X. Qiao, X. Fan, F. Wang, Angew. Chem. 54 (2015) 12788–12790.
[65] Y. Sun, X. Zhu, J. Peng, F. Li, ACS Nano 7 (2013) 11290–11300.
[66] F. Auzel, Chem. Rev. 104 (2004) 139–173.
[67] J.S. Chivian, W.E. Case, D.D. Eden, Appl. Phys. Lett. 35 (1979) 124–125.
[68] X. Li, F. Zhang, D. Zhao, Nano Today 8 (2013) 643–676.
[69] E. Nakazawa, S. Shionoya, Phys. Rev. Lett. 25 (1970) 1710–1712.
[70] L. Tu, X. Liu, F. Wu, H. Zhang, Chem. Soc. Rev. 44 (2015) 1331–1345.
[71] D. Yang, C. Li, G. Li, M. Shang, X. Kang, J. Lin, J. Mater. Chem. 21 (2011) 5923.
[72] Y. Zhang, X. Liu, Y. Lang, Z. Yuan, D. Zhao, G. Qin, W. Qin, J. Mater. Chem. C 3 (2015) 2045–2053.
[73] Y. Zhang, F. Wang, Y. Lang, J. Yin, M. Zhang, X. Liu, D. Zhang, D. Zhao, G. Qin, W. Qin, J. Mater. Chem. C 3 (2015) 9827–9832.
[74] X. Zhai, S. Liu, X. Liu, F. Wang, D. Zhang, G. Qin, W. Qin, J. Mater. Chem. C 1 (2013) 1525.
[75] M. Chen, Y. Ma, M. Li, Mater. Lett. 114 (2014) 80–83.
[76] X. Wang, T. Xu, P. Cai, T. Vu, H.J. Seo, J. Alloys Compd. 691 (2017) 530–536.
[77] B. Zhou, L. Tao, Y.H. Tsang, W. Jin, J. Mater. Chem. C 1 (2013) 4313.
[78] M. Ding, D. Chen, D. Ma, J. Dai, Y. Li, Z. Ji, J. Mater. Chem. C 4 (2016) 2432–2437.
[79] G. Chen, J. Damasco, H. Qiu, W. Shao, T.Y. Ohulchanskyy, R.R. Valiev, X. Wu, G. Han, Y. Wang, C. Yang, H. Agren, P.N. Prasad, Nano Lett. 15 (2015) 7400–7407.
[80] J. Lee, B. Yoo, H. Lee, G.D. Cha, H.S. Lee, Y. Cho, S.Y. Kim, H. Seo, W. Lee, D. Son, M. Kang, H.M. Kim, Y.I. Park, T. Hyeon, D.H. Kim, Adv. Mater. (2017) 29.
[81] X. Wang, R.R. Valiev, T.Y. Ohulchanskyy, H. Agren, C. Yang, G. Chen, Chem. Soc. Rev. 46 (2017) 4150–4167.
[82] X. Wu, Y. Zhang, K. Takle, O. Bilsel, Z. Li, H. Lee, Z. Zhang, D. Li, W. Fan, C. Duan, E.M. Chan, C. Lois, Y. Xiang, G. Han, ACS Nano 10 (2016) 1060–1066.
[83] J. Xu, P. Yang, M. Sun, H. Bi, B. Liu, D. Yang, S. Gai, F. He, J. Lin, ACS Nano 11 (2017) 4133–4144.
[84] W. Zou, C. Visser, J.A. Maduro, M.S. Pshenichnikov, J.C. Hummelen, Nat. Photonics 6 (2012) 560–564.
[85] R. Weissleder, Nat. Biotechnol. 19 (2001).
[86] M.H. Chan, R.S. Liu, Nanoscale 9 (2017) 18153–18168.
[87] B. Liu, C. Li, P. Yang, Z. Hou, J. Lin, Adv. Mater. 29 (2017).
[88] Y.F. Wang, G.Y. Liu, L.D. Sun, J.W. Xiao, J.C. Zhou, C.H. Yan, ACS Nano 7 (2013) 7200–7206.
[89] F. Liégard, J.L. Doualan, R. Moncorgé, M. Bettinelli, Appl. Phys. B 80 (2005) 985–991.
[90] M.J. Weber, Phys. Rev. B 4 (1971) 3153–3159.
[91] J. Shen, G. Chen, A.-M. Vu, W. Fan, O.S. Bilsel, C.-C. Chang, G. Han, Adv. Opt. Mater. 1 (2013) 644–650.
[92] Y. Zhong, G. Tian, Z. Gu, Y. Yang, L. Gu, Y. Zhao, Y. Ma, J. Yao, Adv. Mater. 26 (2014) 2831–2837.
[93] X. Xie, N. Gao, R. Deng, Q. Sun, Q.H. Xu, X. Liu, J. Am. Chem. Soc. 135 (2013) 12608–12611.
[94] X. Cheng, Y. Pan, Z. Yuan, X. Wang, W. Su, L. Yin, X. Xie, L. Huang,Adv. Funct. Mater. 28 (2018), 1800208.
[95] X. Wu, H. Lee, O. Bilsel, Y. Zhang, Z. Li, T. Chen, Y. Liu, C. Duan, J. Shen, A. Punjabi, G. Han, Nanoscale 7 (2015) 18424–18428.
[96] C. Homann, L. Krukewitt, F. Frenzel, B. Grauel, C. Wurth, U. Resch-Genger, M. Haase, Angew. Chem. 57 (2018) 8765–8769.
[97] J. Liu, G. Chen, S. Hao, C. Yang, Nanoscale 9 (2017) 91–98.
[98] Y.-P. Du, X. Sun, Y.-W. Zhang, Z.-G. Yan, L.-D. Sun, C.-H. Yan, Cryst. Growth Des. 9 (2009) 2013–2019.
[99] G. Yi, Y. Peng, Z. Gao, Chem. Mater. 23 (2011) 2729–2734.
[100] B. Shen, S. Cheng, Y. Gu, D. Ni, Y. Gao, Q. Su, W. Feng, F. Li, Nanoscale 9 (2017) 1964–1971.
[101] Z. Li, W. Park, G. Zorzetto, J.S. Lemaire, C.J. Summers, Chem. Mater. 26 (2014) 1770–1778.
[102] X. Chen, L. Jin, W. Kong, T. Sun, W. Zhang, X. Liu, J. Fan, S.F. Yu, F. Wang, Nat. Commun. 7 (2016) 10304.
[103] J.R. Lakowicz, Anal. Biochem. 298 (2001) 1–24.
[104] F. Tam, G.P. Goodrich, B.R. Johnson, N.J. Halas, Nano Lett. 7 (2007) 496–501.
[105] S. Han, R. Deng, X. Xie, X. Liu, Angew. Chem. 53 (2014) 11702–11715.
[106] C. Clarke, D. Liu, F. Wang, Y. Liu, C. Chen, C. Ton-That, X. Xu, D. Jin, Nanoscale 10 (2018) 6270–6276.
[107] A. Priyam, N.M. Idris, Y. Zhang, J. Mater. Chem. 22 (2012) 960–965.
[108] C. Zhang, J.Y. Lee, J. Phys. Chem. C 117 (2013) 15253–15259.
[109] F. Zhang, G.B. Braun, Y. Shi, Y. Zhang, X. Sun, N.O. Reich, D. Zhao, G. Stucky, J. Am. Chem. Soc. 132 (2010) 2850–2851.
[110] E.M. Chan, G. Han, J.D. Goldberg, D.J. Gargas, A.D. Ostrowski, P.J. Schuck, B.E. Cohen, D.J. Milliron, Nano Lett. 12 (2012) 3839–3845.
[111] K.W. Krämer, D. Biner, G. Frei, H.U. Güdel, M.P. Hehlen, S.R. Lüthi, Chem. Mater. 16 (2004) 1244–1251.
[112] G.A. Sotiriou, M. Schneider, S.E. Pratsinis, J. Phys. Chem. C Nanomater. Interfaces 115 (2011) 1084–1089.
[113] F. Wang, Y. Han, C.S. Lim, Y. Lu, J. Wang, J. Xu, H. Chen, C. Zhang, M. Hong, X. Liu, Nature 463 (2010) 1061–1065.
[114] F. Wang, X. Liu, J. Am. Chem. Soc. 130 (2008) 5642–5643.
[115] F. Zhang, Q. Shi, Y. Zhang, Y. Shi, K. Ding, D. Zhao, G.D. Stucky, Adv. Mater. 23 (2011) 3775–3779.
[116] H.S. Qian, Y. Zhang, Langmuir: ACS J. Surf. Colloids 24 (2008) 12123–12125.
[117] C. Zhang, L. Yang, J. Zhao, B. Liu, M.Y. Han, Z. Zhang, Angew. Chem. 54 (2015) 11531–11535.
[118] J. Lai, Y. Zhang, N. Pasquale, K.B. Lee, Angew. Chem. 53 (2014) 14419–14423.
[119] R. Deng, F. Qin, R. Chen, W. Huang, M. Hong, X. Liu, Nat. Nanotechnol. 10 (2015) 237–242.
[120] B. Chen, Y. Liu, Y. Xiao, X. Chen, Y. Li, M. Li, X. Qiao, X. Fan, F. Wang, J. Phys. Chem. Lett. 7 (2016) 4916–4921.
[121] L. Wang, H. Dong, Y. Li, C. Xue, L.D. Sun, C.H. Yan, Q. Li, J. Am. Chem. Soc. 136 (2014) 4480–4483.
[122] D. Chen, Y. Yu, P. Huang, F. Weng, H. Lin, Y. Wang,Appl. Phys. Lett. 94 (2009), 041909.
[123] Y. Dwivedi, S.B. Rai, Opt. Mater. 31 (2009) 1472–1477.
[124] G.S. Maciel, P.N. Prasad, Opt. Mater. 178 (2000) 65–69.
[125] X. Wang, X. Yan, C. Kan, J. Lumin. 131 (2011) 2325–2329.
[126] Q. Su, S. Han, X. Xie, H. Zhu, H. Chen, C.K. Chen, R.S. Liu, X. Chen, F. Wang, X. Liu, J. Am. Chem. Soc. 134 (2012) 20849–20857.
[127] R. Chen, V.D. Ta, F. Xiao, Q. Zhang, H. Sun, Small 9 (2013) 1052–1057.
[128] L. Cheng, K. Yang, M. Shao, S.-T. Lee, Z. Liu, J. Phys. Chem. C 115 (2011) 2686–2692.
[129] Z. Li, Y. Zhang, S. Jiang, Adv. Mater. 20 (2008) 4765–4769.
[130] L. Zhou, R. Wang, C. Yao, X. Li, C. Wang, X. Zhang, C. Xu, A. Zeng, D. Zhao, F. Zhang, Nat. Commun. 6 (2015) 6938.
[131] B. Del Rosal, D.H. Ortgies, N. Fernandez, F. Sanz-Rodriguez, D. Jaque, E.M. Rodriguez, Adv. Mater. 28 (2016) 10188–10193.
[132] K.Y. Zhang, Q. Yu, H. Wei, S. Liu, Q. Zhao, W. Huang, Chem. Rev. 118 (2018) 1770–1839.
[133] W. Zheng, D. Tu, P. Huang, S. Zhou, Z. Chen, X. Chen, Chem. Commun. 51 (2015) 4129–4143.
[134] Y. Lu, J. Zhao, R. Zhang, Y. Liu, D. Liu, E.M. Goldys, X. Yang, P. Xi, A. Sunna, J. Lu, Y. Shi, R.C. Leif, Y. Huo, J. Shen, J.A. Piper, J.P. Robinson, D. Jin, Nat. Photonics 8 (2013) 32–36.
[135] Y. Wang, R. Deng, X. Xie, L. Huang, X. Liu, Nanoscale 8 (2016) 6666–6673.
[136] D. Chen, M. Xu, M. Ma, P. Huang, J. Chem. Soc. Dalton Trans. 46 (2017) 15373–15385.
[137] L. Zhou, Y. Fan, R. Wang, X. Li, L. Fan, F. Zhang, Angew. Chem. 57 (2018) 12824–12829.
[138] Y. Fan, P. Wang, Y. Lu, R. Wang, L. Zhou, X. Zheng, X. Li, J.A. Piper, F. Zhang, Nat. Nanotechnol. 13 (2018) 941–946.
[139] A.R. Hong, Y. Kim, T.S. Lee, S. Kim, K. Lee, G. Kim, H.S. Jang, ACS Appl. Mater. Interfaces 10 (2018) 12331–12340.
[140] Q. Ju, D. Tu, Y. Liu, R. Li, H. Zhu, J. Chen, Z. Chen, M. Huang, X. Chen, J. Am. Chem. Soc. 134 (2012) 1323–1330.
[141] Y. Wu, D. Li, F. Zhou, H. Liang, Y. Liu, W. Hou, Q. Yuan, X. Zhang, W. Tan, Chem. Sci. 9 (2018) 5427–5434.
[142] Y. Liu, K. Ai, J. Liu, Q. Yuan, Y. He, L. Lu, Angew. Chem. 51 (2012) 1437–1442.
[143] Z. Liu, Z. Li, J. Liu, S. Gu, Q. Yuan, J. Ren, X. Qu, Biomaterials 33 (2012) 6748–6757.
[144] G. Tian, X. Zheng, X. Zhang, W. Yin, J. Yu, D. Wang, Z. Zhang, X. Yang, Z. Gu, Y. Zhao, Biomaterials 40 (2015) 107–116.
[145] Y. Sun, M. Yu, S. Liang, Y. Zhang, C. Li, T. Mou, W. Yang, X. Zhang, B. Li, C. Huang, F. Li, Biomaterials 32 (2011) 2999–3007.
[146] S. He, N.J.J. Johnson, V.A. Nguyen Huu, E. Cory, Y. Huang, R.L. Sah, J.V. Jokerst, A. Almutairi, Nano Lett. 17 (2017) 4873–4880.
[147] Y. Li, Y. Gu, W. Yuan, T. Cao, K. Li, S. Yang, Z. Zhou, F. Li, ACS Appl. Mater. Interfaces 8 (2016) 19208–19216.
[148] Y. Wang, S. Song, J. Liu, D. Liu, H. Zhang, Angew. Chem. 54 (2015) 536–540.
[149] X. Li, L. Zhou, Y. Wei, A.M. El-Toni, F. Zhang, D. Zhao, J. Am. Chem. Soc. 137 (2015) 5903–5906.
[150] W. You, D. Tu, W. Zheng, X. Shang, X. Song, S. Zhou, Y. Liu, R. Li, X. Chen, Nanoscale 10 (2018) 11477–11484.

**Yong Fan** received his BS degree (2009) from Xi'an Jiaotong University and PhD (2015) from Tsinghua University (China). Since then he has studied as a postdoctoral fellow at Fudan University. His current research interests focus on design and synthesis of functional inorganic nanomaterials and optical devices for bio-applications.

**Lu Liu** received his MS degree (2015) from Jilin University (China). He is currently a PhD candidate under the direction of Professor Fan Zhang in the Chemistry Department of Fudan University, China. His current research involves multifunctional nanomaterials synthesis and bio-applications of luminescent nanomaterials.

**Prof. Fan Zhang** received his PhD in 2008 from Fudan University followed by more than 2 years postdoctoral experience in University of California at Santa Barbara before joining as a professor in the Chemistry Department of Fudan University in 2010. His current research interests include bioanalysis, bioimaging, drug delivery and disease therapy. Prof. Zhang has authored a number of book chapters, patents and more than 100 peer-reviewed research papers in international journals i.e. Nat. Nanotech.,Nat. Commun., J. Am. Chem. Soc., Angew. Chem. Int. Ed., Adv. Mater., and authored 2 English books.